J Math Chem (2010) 47:1366–1419
DOI 10.1007/s10910-010-9662-x

REVIEW PAPER

Review of theories on ionization in fast ion-atom collisions with prospects for applications to hadron therapy

Dževad Belkić

Received: 20 December 2009 / Accepted: 8 February 2010 / Published online: 11 March 2010
© Springer Science+Business Media, LLC 2010

Abstract This study emphasizes the need for a systematic and in-depth connection between the progress in quantum theory of energetic ion collisions and applications to hadron therapy. Scattering theory for fast ion beams has reached its stage of development where accurate and robustly applicable methodologies can advantageously be exported to applied fields such as space research, fusion energy program, medicine, etc. In particular, distorted wave collision theories at high energies readily provide total, partial and fully differential cross sections for inelastic collisions of ionic projectiles with any target system. By numerous and thorough testings, such theoretical cross sections were found to exhibit excellent agreement with experimental data on atomic targets. Adequate extensions of these methods to molecular targets were also accomplished with computational efforts that are approximately comparable to that for multi-electron atomic targets. This was done by using the standard Slater-type atomic basis functions for any molecular targets, including tissue-equivalent materials (e.g. water) of relevance to hadron therapy. This expertize needs to be brought to medicine through ion transport physics, which most frequently employs the crude Bragg sum rule for obtaining molecular cross sections as linear combination of atomic cross sections. Relativistic distorted wave theories are also available, but not currently in use for modeling the passage of relativistic ions through tissue, as needed in hadron therapy of deep-seated tumors. It is high time for extensive and thorough applications of the well-established distorted wave scattering theories to fast collisions of bare and partially clothed multiple charged ions with water molecule. This type of application would provide the most accurate data bases for various cross sections (on electron capture, excitation, ionization, etc) that can be used as reliable entry data for subsequent Monte Carlo simulations of energy losses of ions during their passage

Dž. Belkić (✉)
Karolinska Institute, P.O. Box 260, 171 76 Stockholm, Sweden
e-mail: Dzevad.Belkic@ki.se

through tissue. In order to gain in overall efficiency, these theoretical cross sections could be precomputed at sufficiently dense multi-variable grids, thus yielding modules for advantageous direct sampling during stochastic simulations. Such a comprehensive strategy could provide both accurate and efficient algorithms that would incorporate the state-of-the-art methodologies from high-energy atomic scattering theory involving ion beams. This is currently missing in the physics part of hadron therapy, since all the major Monte Carlo codes customarily employ atomic cross section data bases that rely almost exclusively upon the Bethe–Bloch formula and some phenomenological expressions with fitting parameters adjusted to the limited sets of experimental data. Crucially, the need is emphasized for the introduction of a still missing Monte Carlo code which could simulate transport of ions together with secondary electrons in tissue. The current main Monte Carlo codes simulate transport of either ions or electrons, but not both simultaneously. However, energetic ions produce a large number of electrons by densely ionizing the traversed tissue and many of them are δ-electrons i.e. capable on their own of ionizing various targets. Due to their light mass and considerable energy, δ-electrons undergo multiple scatterings. Because of this cumulative effect, among all the double strand breaks of DNA molecules of tissue treated by ion therapy, some 70% are produced by δ-electrons. Hence the necessity to simulate transport of δ-electrons produced by primary ion beams. Such types of computations are presently missing from the major ion transport codes. Overall, this work thoroughly analyzes conceptual and computational advances of the leading quantum-mechanical distorted wave theories for energetic ion collisions aimed at applications to medicine. Additionally, the main strategic directions are also indicated to further cross-disciplinary fertilization between medicine and basic research on collision theory of fast heavy ions of relevance to hadron therapy.

Keywords Ionizing collisions · Distorted wave theories · Radiotherapeutic ions · Hadron therapy

1 Introduction

The atomic physics research field of high-energy collisions of ions with matter provides its versatile data bases (cross sections, rate coefficients) to other branches of physics (astrophysics, plasma physics, particle transport physics) and applied disciplines (fusion, radiotherapy, radiation protection in manned space missions), etc. Such data describe various inelastic scattering events, including electron capture (also called electron transfer and charge exchange), excitation, electron loss (projectile ionization), ionization (target ionization) and their combinations (transfer excitation, transfer ionization, loss-excitation, loss-ionization, etc) [1–5]. Probabilities for multiple electron transitions are enhanced for the increased nuclear charge of projectiles. Multiply charged nuclei are used as radiotherapeutic ions. They are also employed as a new source of energy in tokamacs as high-temperature thermonuclear reactors. Here, ionic plasma needs to be maintained for a sufficiently long period of time against its natural neutralization tendencies in collisions of nuclei with materials from the tokamac walls. Powerful, multifaceted techniques involving heavy ions have been

developed for plasma diagnostics ranging from charge exchange spectroscopy via determination of energy losses in radiative and radiationless collisions for identification of specific elements from the tokamac walls with the highest probabilities for plasma neutralization by electron capture. Thermonuclear plasma stability cannot be achieved unless the major aspects of atomic interactions involving ions are thoroughly examined theoretically and verified experimentally. Both sets of the mentioned data, those for single- and multiple-electron transitions, need to be very accurate as the input data for subsequent stochastic simulations that ingrain deterministic cross sections for fast ion-atomic collisions in various applications. These data from atomic collisions of ions with matter can be obtained from theories and measurements. A variety of such experimentally determined and theoretically predicted cross sections has extensively been accumulated in the literature particularly over the last three decades [3,4].

In exhaustive comparisons with measurements, past experience conclusively established that the most adequate quantum-mechanical theory for high-energy ion-atom collisions is the continuum distorted wave (CDW) method [6–9] which is valid in the region slightly above the Massey resonance peak [10]. The name of this method comes from correlating the projectile with the target through the allowance of electronic continuum intermediate states that act as a distortion in the total scattering wave function of the whole system. For example, in the entrance channel, the active electron is simultaneously bound to the target nucleus and free in the field of the projectile nucleus. Therefore, in the initial state of the system, the distortion associated with continuum intermediate states of the active electron stems from the Coulomb wave function centered on the impinging nuclear charge. Distorted waves are of especially critical importance to the exit channel for ionizing collisions, as they describe the so-called two-center effects [8] that are completely missing from the first Born (B1) [11–15] and the Bethe–Bloch [16,17] approximations. The two-center effects include intermediate stages of collision and describe active electrons as propagating in the Coulomb fields of the projectile and target nuclei. Thus, in ionization of a target, the B1 approximation employs only one full Coulomb wave function centered on the target nucleus in the exit channel for the final scattering state Ψ_f^-, whereas the electron motion in the projectile field is inadequately described by a plane wave [11–15]. By contrast, the CDW method describes the whole ionization collision in a more physically adequate manner by using three Coulomb wave functions. Two of these latter wave functions are for the electronic motions and they are centered on the projectile and target nuclei for Ψ_f^-. The third Coulomb wave describes the relative motion of the two heavy nuclei. The physical significance of the additional Coulomb electronic wave function in the CDW method for ionization is in leading to a new source for production of emitted electrons due to an extra mechanism called electron capture to continuum (ECC) of the projectile. Here, the electron is considered as being "captured" by the projectile albeit not in a bound, but rather in a continuum state. Through this mechanism, which has been experimentally detected in single ionization [18–41], the projectile and electron travel together in the same direction with nearly equal velocities vectors $\boldsymbol{v}$ and $\boldsymbol{\kappa}$, respectively ($\boldsymbol{\kappa} \approx \boldsymbol{v}$). This is recognized as a resonance effect (hence the resulting enhanced cross sections), which is manifested in an asymmetric cusp-shaped angular distribution for the forward emitted electrons. The description of the exit channel for ionization in the B1 approximation could be roughly

satisfactory only for very slow ejected electrons, that are near the target nucleus and simultaneously far away from the nucleus of the projectile. Note that the cusp mechanism has also been observed experimentally in solid state targets and in this area the name "convoy electrons" is interchangeably used for ECC electrons [23]. This latter name stems from the circumstance that ECC electrons are aligned with and accompanied by scattered projectiles as reminiscent of a convoy-like moving away from the target rest. Emitted slow electrons provide the major contribution to the total cross sections. However, for thorough studies of collisional dynamics, it is imperative to look beyond total (integrated) cross sections to describe properly the differential cross sections that give the energy and angular distributions of electrons ionized from the target [8,44,45]. Both these distributions manifestly exhibit the two-center effect. The other two mechanisms for production of δ-electrons are the emissions leading to the forward and binary peaks (both described by the CDW and B1 methods). The forward emission occurs at a zero-valued angle of the ejected electron, $\theta_e \approx 0$. The binary encounter (BE) peak corresponds to $\kappa \approx 2v\cos\theta_e$.

The most remarkable feature of an interplay between the BE and ECC mechanisms of ionization is manifested when passing from single to multiple ionization in the case of non-hydrogenic targets. This has recently been evidenced in experimental measurements of doubly differential cross sections for single and multiple ionization of Ar by H^+ [28,29] as well as of He, Ne and Ar by $F^{8+,9+}$ and $I^{23+,26+}$ [30–32]. The ECC cusp effect involving two-electron continua was studied via simultaneous electron loss (projectile ionization) and target ionization in He–He collisions [40,41]. The striking observation reported in [28–32] is that the ECC cusp can become even dominant over the BE peak for ionization. Specifically, the coincidence experiment of Afrosimov et al. [29] (simultaneous measurements of double differential cross sections for near-forward-cone ejected electrons and charge state of the target rest) demonstrated that the BE electrons were produced almost entirely by single ionization of Ar by protons. Moreover, determination of the position of the BE peak in coincidence with detection of single-charged recoil ions showed that the emitted BE electrons stem from the valence M-shell of Ar. Among all the electron orbital velocities of Ar, the one which is associated with the M-shell of this atom matches most closely the condition $v_e \approx 2v$ for the forward emitted BE electrons ($\cos\theta_e \approx 1$). Furthermore, in the same experiments [28,29], the group of ECC electrons was found to be significant only when detected in coincidence with multiple charged argon ions Ar^{k+} ($k = 2, 3, 4, \ldots$), whereas totally negligible counts were recorded for Ar^+. In other words, the ECC electrons become a dominant mechanism for multiple ionization. To see from which target shell these electrons were emitted, it is sufficient to compare the binding electronic energies of various shells in Ar and find the level which matches best the ejected electron energy from the ECC peak at which the orbital electron velocity equalizes the projectile speed ($v_e \approx v, \cos\theta_e \approx 0$). This was found to be the L-shell energy of Ar [28,29]. Here, it is pertinent to emphasize certain remarkable similarities between the experimental data for ionization [29] and charge exchange [42]. Thus e.g. the charge-state distributions near the ECC peak was estimated to be 13, 42, 37, and 8% for the charge states 1+, 2+, 3+ and 4+, respectively [29]. This is very close to the corresponding charge-state distributions 13, 50, 30, and 7% for the same charge states 1+, 2+, 3+ and 4+ for charge exchange [42]. The direct

implication of the findings from the experiments reported in [28–32] is that theories for multiple ionization must include the two-center effect in order to account properly for emission of fast electrons that are predominantly from the ECC source. Overall, these experiments with non-hydrogenlike atomic targets prove that the BE and ECC electrons play a remarkably complementary role as they appear to be generated by two completely different mechanisms (single and multiple ionization) and originate from the two well-separated target energy levels (outer and inner shells). Thus, while for single ionization the ECC mechanism is conspicuous, it became inconspicuous for multiple ionization. Single ionization is associated with slow electrons from the one-center BE mechanism which is a direct collision of the projectile and the target active electron, such that the target nucleus and the remaining electrons are considered as being passive as if they were spectators. On the other hand, multiple ionization is mediated by fast electrons due to the ECC mechanism which necessitates two centers thus activating both the projectile and target nucleus. As opposed to a single collision (projectile nucleus—target electron) in the BE effect, a double collision of the active electron on the projectile and target nucleus is required to produce the ECC cusp, as reminiscent of the Thomas billiard-type two successive elastic encounters occurring in capture of an electron from the target by an energetic projectile. This type of correlation between electron capture and ionization permits obtaining the same angular distributions in a given theory for the Thomas peak in charge exchange by using the corresponding ionization transition amplitude in the vicinity of the ECC cusp [43].

In the CDW method [8], the distortions due to electronic continuum intermediate states are properly included in the entrance and exit channels. Nevertheless, the corresponding full Coulomb wave function within the initial scattering state was found in applications to lead to overestimation of experimentally measured total cross sections near and below the Massey peak. Typically, all total cross sections computed by the CDW method keep on rising as the impact energy E decreases, whereas the corresponding experimental data generally decline in the same region exhibiting the Massey peak. This bending of the curve for the total cross sections can also be obtained within the CDW methodologies if the full Coulomb wave function for the distortion of the initial state in the entrance channel is approximated by its long range asymptotic eikonal form. The resulting simplification of the CDW method is acronymed as CDW-EIS [46], where EIS stands for the initial eikonal state. In this way, the Massey peak is systematically reproduced by the CDW–EIS method, leading to quantitative agreement with measurements, as reviewed in [47,48]. Another autonomous derivation of an eikonal version of the CDW method is provided by the modified Coulomb–Born (MCB) approximation [49,50]. The MCB method does not start from the CDW method to introduce its simplified variant in the form of the CDW–EIS approximation, as originally done by Crothers and McCann [46]. Rather, the MCB method was derived without any reliance upon the CDW method. Yet the MCB and CDW methods share precisely the same description for the final total scattering state. They differ in the initial scattering state, where the MCB method uses the ansatz in the form of the logarithmic Coulomb phase factor for the electronic continuum intermediate states. With such an ansatz, the perturbation potential in the entrance channel is unequivocally defined by the application of the operator $H - E$ onto the

initial state in the matrix element for the prior form of the transition amplitude T_{if}^{-}. Here, H and E are the full Hamiltonian and the total energy of the whole system (projectile plus target). Of course, since the same Coulomb eikonal phase factor is used in the MCB and CDW–EIS methods (irrespective of whether or not this phase factor is introduced in the MCB method from the onset as an ansatz distortion function or encountered in the CDW–EIS method as a result of approximating the full Coulomb wave from the CDW method), the prior transition amplitude in the MCB and CDW–EIS approximations coincide with each other. The CDW, CDW–EIS and MCB methods are computationally attractive since the fully analytical expressions are available for the transition amplitudes for inelastic collisions involving one active electron. We shall illustrate the performance of several among a wider class of the CDW methodologies applied to ionizing collisions involving positively and negatively charged heavy projectiles and targets, respectively. The complementary illustrations of this successful theoretical framework for collisions of positively charged projectiles and either neutral targets or positively charged ions are abundantly available in the literature [3,4,47,48].

Atomic units should be used throughout unless otherwise stated.

2 Ionizing collisions and distorted wave theories

Ionizing collisions involve bound-free transitions of the active electron. For this reason ionization is very different from excitation and electron capture in which bound-bound electronic transitions take place. As a result, single ionization leads to three particles in the exit channel. In excitation and electron capture, two particles are present in both the entrance and exit channels. Having three particles in the exit channel for ionization renders the boundary condition problem more difficult to fulfill than for excitation and electron capture. The boundary condition problem necessitates that the following two requirements are simultaneously fulfilled: (a) the scattering wave functions $\Psi_{i,f}^{\pm}$ of the whole system in the initial and final states must satisfy the correct asymptotic behaviors at large inter-particle distances in the corresponding entrance and exit channel, and (b) the associated perturbation potentials $V_{i,f}$ in the post/prior transition amplitudes $T_{i,f}^{\pm}$ ought be of short range and consistent with $\Psi_{i,f}^{\pm}$. Short-range potentials, that decay faster than $1/r$ as the distance r becomes infinitely large, are necessary to assure that no interaction takes place in the asymptotic region in which the scattering event is viewed as completed. For ionization, the large distances assume that all three particles are infinitely separated from each other. However, for fuller adequacy of the description of a scattering event, it is also important to account for the contribution to the transition amplitude from finite inter-particle separations. At finite distances, correlation effects between the projectile and the target are likely to play a significant role. Therefore, the task is to simultaneously fulfill the proper boundary conditions at asymptotic distances and include the projectile-target correlations. These latter two effects should cohere with each other, such that the allowance for correlations does not impede the correct boundary conditions. This can be achieved with a high degree of flexibility by resorting to the distorted wave formalism of scattering. In this formalism, the perturbation interactions $V_{i,f}$ are modified by the introduction of certain distorting

potentials $W_{i,f}(R)$. The modified perturbation potentials are given by the difference $V_{i,f} - W_{i,f}(R)$. The additional potentials $W_{i,f}(R)$ remove any remaining asymptotic Coulomb potentials $V_{i,f}(R)$ from $V_{i,f}$ at large values of the inter-aggregate separation R, which is basically the internuclear distance. In this way, the new perturbation potential $V_{i,f} - W_{i,f}(R)$ is of a short range in the limit $R \longrightarrow \infty$, as it should be according to the requirements from the correct boundary conditions. The physics of rearranging collisions is not changed by the distortions $W_{i,f}(R)$, since these can lead exclusively to elastic collisions due to their dependence upon R alone. However, being dependent solely upon R makes the potentials $W_{i,f}(R)$ incapable of introducing the correlation effects that would encompass the interactions between the projectile and the active target electrons. This can be successfully remedied by adopting a special variant of the distorted wave formalism developed by Dodd and Greider [51]. Here, an intermediate channel "x" is introduced with its channel potential V_x which is able to correlate the projectile with the target electrons that participate actively in the transition. Such a procedure, in fact, models the exact full Schrödinger equation for $\Psi_{i,f}^{\pm}$ by its corresponding distorted wave Schrödinger equation for the approximate solutions $\chi_{i,f}^{\pm}$ for the total scattering states. These two Schrödinger equations are linked by the requirement that $\Psi_{i,f}^{\pm}$ and $\chi_{i,f}^{\pm}$ possess the same correct asymptotic behaviors and have the joint proper perturbation potentials that cause the transition in the investigated collision. The proper asymptotes $\Phi_{i,f}^{\pm}$ of $\Psi_{i,f}^{\pm}$ are given by the product of the undistorted channel states $\Phi_{i,f}$ and the logarithmic Coulomb phase factors from the long range remainders $V_{i,f}(R)$ of $V_{i,f}$. These latter phases themselves are the asymptotic forms of the full Coulomb wave functions for $V_{i,f}(R)$. With a judicious choice of the model potential V_x, the distorted wave Schrödinger equation can be solved to a good approximation. One of the solutions for the distorted wave functions in the first-order approximation to the Dodd–Greider series expansion for the transition amplitude expresses $\chi_{i,f}^{\pm}$ as the product of $\Phi_{i,f}$ and the associated projectile-target correlation functions $\mathcal{L}_{i,f}^{\pm}$ with the correct asymptotes $\chi_{i,f}^{\pm} = \Phi_{i,f}^{\pm}\mathcal{L}_{i,f}^{\pm} \longrightarrow \Psi_{i,f}^{\pm} \longrightarrow \Phi_{i,f}^{\pm}$ as $R \rightarrow \infty$. For excitation and electron capture, the correlation functions $\mathcal{L}_{i,f}^{\pm}$ are the products of the Coulomb wave functions for the relative motion of the heavy nuclei and the Coulomb wave functions of the active electron in the field of the projectile or target nucleus in the entrance and exit channel, respectively. Hence the name C2 (two Coulomb) wave functions for excitation and electron capture. For ionization, one more Coulomb wave function appears in the product for the correlation function $\mathcal{L}_f^-$ in the exit channel because the emitted electron is free simultaneously in the fields of both the projectile and target nuclei. This leads to the so-called C3 (three Coulomb) wave function for ionization, as first derived by Belkić in 1978 [8] from the distorted wave Schrödinger equation in the case of ionization of a hydrogenlike atomic system by a bare nucleus. The C3 wave function takes into account the two-center effect i.e. the ECC mechanism.

It should be recalled that the B1 model employs the unperturbed initial and final channel states Φ_i and Φ_f weighted with the perturbation potential V_i in the transition matrix element in the prior form, T_{if}^-. Here, the initial state Φ_i in the entrance channel is given by the product of the bound state wave function of the target and the plane wave of the relative motion of the scattering heavy aggregates (projectile and target).

The final state Φ_f in the exit channel is described in the B1 approximation by the product of the Coulomb wave function of the ejected electron in the field of the target nuclear charge with the plane wave of relative motion of heavy particles. The latter product additionally includes the bound state wave function of the target remainder in the case of a multi-electron target. This description in the B1 approximation for an ionizing collision assumes that the emitted electron is influenced solely by the field of its parent nucleus. Such an assumption could approximately be satisfactory for high-energy total cross sections that are determined predominantly by small momenta of the ejected electrons. Of course, even total cross sections in the B1 approximation are inadequate near and below the Massey peak.

3 Main features of CDW methodologies for ionization

As stated, the correct boundary conditions are essential for ionization which can be exemplified by the following pure three-body collisional problem:

$$Z_P + (Z_T, e)_i \longrightarrow Z_P + Z_T + e, \tag{3.1}$$

where the parentheses symbolize the bound states. Hereafter, Z_P and Z_T are the projectile and target nucleus, respectively. We also emphasize that it is more difficult to fulfill the correct boundary conditions for ionization (3.1) than for the corresponding electron capture process:

$$Z_P + (Z_T, e)_i \longrightarrow (Z_P, e)_f + Z_T. \tag{3.2}$$

This difficulty stems from the appearance of three charged particles in the exit channel of ionization (3.1) as opposed to only two free particles in electron capture (3.2). The principal objective is to approximately solve the total Schrödinger equation for the scattering wave function of the final state Ψ_f^- by preserving the known exact asymptotic behavior at infinitely large separations among the three free charged particles. The known asymptotic form of the exact wave function for the three free charged particles is given by the product of three Coulomb-distorted plane. A Coulomb-distorted plane wave is the usual plane wave multiplied by the appropriate logarithmic Coulomb phase factor. As such, three multiplicative Coulomb logarithmic phase distortions of the product of three plane waves appear in the exact asymptotic final wave function for the exit channel in process (3.1). This exact Coulomb boundary condition for the final state in ionization (3.1) was first satisfied by Belkić [8] who derived the C3 function from the complete Schrödinger equation in the distorted wave formalism. This latter asymptotic form has previously been reported by Rosenberg [52] and attributed to an unpublished result of Redmond. However, Rosenberg has not given any derivation of Redmond or anybody else. By reference to Messiah [53], who cited the well-known formula for two Coulomb-distorted plane waves, Rosenberg [52] merely wrote a generalized product of n Coulomb logarithmic phase factors for n free charged particles, but this was not derived from any equation. By contrast, Belkić [8] started from the full Schrödinger equation which gave the C3 wave

function whose asymptotic behavior reduces to the product of three Coulomb-distorted plane waves. These three Coulomb waves from the C3 wave function have the Sommerfeld parameters $Z_P Z_T/v$, $Z_P/|\boldsymbol{\kappa} - \boldsymbol{v}|$ and Z_T/κ stemming from the pairwise separate interactions $Z_P - Z_T$, $Z_P - e$ and $Z_T - e$, respectively. Hereafter, $\boldsymbol{\kappa}$ and $\boldsymbol{p} = \boldsymbol{\kappa} - \boldsymbol{v}$ are the electron momentum vectors in the target and projectile frame, respectively.

In the same investigation of Belkić [8], the correct boundary condition was also fulfilled in the entrance channel for ionization (3.1). This is manifested in the solution of the full distorted wave Schrödinger equation for Φ_i^+ given by the product of the target bound state and the C2 function. This C2 function is the product of two full Coulomb waves for electron e and nucleus Z_T, each centered on the projectile nuclear charge Z_P. Of course, the same distorted wave treatment of the entrance channel is also used for three-body electron capture (3.2).

The resulting theory from the study by Belkić [8] represents the CDW-3B method with the correct boundary conditions in the entrance and exit channels of ionization in the general three-body process (3.1). Similarly to electron capture (3.2) described via the CDW-3B method, the transition amplitude for ionization (3.1) in the same theory possesses the product of the initial and final Coulomb waves for the relative motion of the two nuclei as the whole contribution from the inter-nuclear potential $V_{PT} = Z_P Z_T/R$. The well-known eikonal result for this latter product is the standard phase factor $(\mu v \rho)^{2iZ_P Z_T/v}$, which disappears altogether from the total cross section $Q_{if}^{(\mathrm{CDW-3B})}$ for processes (3.1) and (3.2). Here, ρ is the quantum-mechanical equivalent of the classical impact parameter, whereas μ is the reduced mass of the projectile and target nuclei. Therefore, the inter-nuclear potential V_{PT} yields no contribution to the total cross section $Q_{if}^{(\mathrm{CDW-3B})}$ for ionization in the mass limit $M_P \gg 1$ and $M_T \gg 1$ which is justified for (3.1) and (3.2). This holds true for all ion-atom collisions that involve heavy nuclei [7]. Such a finding from the CDW-3B method stems from the symmetric treatment of the relative motion of the projectile and target nucleus in the entrance and exit channels.

Regarding the ejected electron e, the C3 wave function takes into account the presence of the two Coulomb centers located at the nuclear charges Z_P and Z_T. This describes the emitted electron moving simultaneously in the field of Z_P and Z_T thus yielding the two-center effect. For $\kappa \ll v$, the electron is mainly near its parent nucleus Z_T. Such small values of electron momentum κ (soft electrons) give the major contribution to total cross sections at high energies. The influence of the other Coulomb center, Z_P, becomes dominant for the electrons ejected nearly in the direction of the scattered projectiles ($\boldsymbol{\kappa} \approx \boldsymbol{v}$). These electrons are considered as being 'captured' by Z_P in a continuum state via the ECC effect. Additionally, the CDW-3B method gives the forward and binary effects in the angular distributions of scattered projectiles Z_P. The forward effect appears as a peak near zero emission angle $\theta_e \approx 0$ in the differential cross sections for the emitted electrons. Likewise, the binary effect is manifested as a peak when $v_e \approx 2v \cos\theta_e$, as mentioned. The forward, ECC and binary peaks have been detected experimentally and found to be in quantitative agreement with the cross sections predicted by the CDW-3B method of Belkić [8]. Importantly, the CDW-3B method is computationally attractive, because the transition amplitude $T_{if}^{(\mathrm{CDW-3B})}$ for process

(3.1) was derived in [8] in a purely analytical, closed form. As in charge exchange, the CDW-3B method for ionization overestimates the experimentally measured total cross sections at lower impact energies below and close to the Massey peak [10]. This is mainly due to the presence of the normalization constant $N^+(\nu_P) \equiv N^+(Z_P/v)$ of the electronic full Coulomb wave function in the entrance channel. The normalization factor $|N^+(Z_P/v)|^2 = (2\pi Z_P/v)/[1 - \exp(-2\pi Z_P/v)]$ is augmented with decreasing incident velocity v. As such, the scaled cross sections $Q_{if}^{(\mathrm{CDW-3B})}/|N^+(Z_P/v)|^2$ will be significantly reduced below the Massey peak [10] in comparison with $Q_{if}^{(\mathrm{CDW-3B})}$. The normalization $N^+(Z_P/v)$ disappears when the mentioned full Coulomb wave from the CDW-3B method is approximated by its asymptotic form. Such a simplification of the CDW-3B method [8] yields the CDW-EIS-3B method proposed by Crothers and McCann in 1983 [46]. Overall, the CDW-3B and CDW-EIS-3B methods have the same final scattering state and the gradient-gradient ($\nabla \cdot \nabla$) perturbation in the transition amplitude. These two methods differ only in describing the entrance channel, where the CDW-EIS-3B method simplifies the CDW-3B method via the replacement of the full Coulomb wave function by its asymptotic form, which is the associated logarithmic phase factor. As anticipated from the mentioned behavior of the scaled cross sections $Q_{if}^{(\mathrm{CDW-3B})}/|N^+(Z_P/v)|^2$, explicit computations confirm that around and below the Massey peak [10], the results for $Q_{if}^{(\mathrm{CDW-EIS-3B})}$ are always considerably smaller than the related theoretical data $Q_{if}^{(\mathrm{CDW-3B})}$. This circumstance leads to an improved agreement between theory and measurement at intermediate and lower energies.

In a study from 1980 related to the same process (3.1), Garibotti and Miraglia [54] rederived the C3 wave function of Belkić [8] in the exit channel. However, they ignored the correct boundary condition in the entrance channel where merely the undistorted wave function Φ_i was used. Thus, their so-called multiple scattering (MS) model[1] as a whole is inadequate, since it neglects the correct boundary conditions that must be simultaneously satisfied in the entrance and exit channels [7,8]. Yet another conceptual error exists in the MS method [54–56] consisting of a non-vanishing contribution to the total cross section Q from the inter-nuclear potential $V_{PT} = Z_P Z_T/R$, which yields the mentioned Coulomb wave function for the relative motion of Z_P and Z_T. This latter Coulomb wave is one of the three Coulomb waves from the C3 wave function of Belkić [8] in the exit channel of process (3.1). In contrast to the MS method [54], the inter-nuclear potential V_{PT} completely disappears from the total cross section in the CDW-3B method [8]. First, this occurs because of multiplication of two Coulomb waves for the relative motions of nuclei Z_P and Z_T from the entrance and exit channel, so that in the end only the phase factor $(\mu v \rho)^{2iZ_P Z_T/v}$ persists, as the whole remainder of the effect from V_{PT} upon the transition amplitude. Second, the phase $(\mu v \rho)^{2iZ_P Z_T/v}$ vanishes from the total cross section in the CDW-3B method, pointing to a zero contribution of the inter-nuclear potential V_{PT} to $Q_{if}^{(\mathrm{CDW-3B})}$. Moreover, in addition to

[1] The term 'multiple scattering' for the model from [54] presumably stems from employing the Coulomb wave for the relative motion of heavy nuclei in the exit channel in lieu the corresponding plane wave from the B1 approximation for the same motion.

its basic theoretical defects, the MS model [54] is computationally demanding, since its transition amplitude cannot be calculated analytically, in contrast to the CDW-3B method [8]. In order to partially mitigate this drawback, Garibotti and Miraglia [54] approximated their T-matrix element by an expression derived from the additional peaking approximation.[2]

Of late, the C3 wave function has been reinvented by Brauner et al. [62] and others [63–68]. Specifically, Brauner et al. [62] adapted the derivation of the C3 wave function of Belkić to ionization of atoms by electron impact, but without due citation of the original work [8]. Moreover, the adaptation from [62] represents a trivial specification of the required masses. This obvious specification could have been done directly in the already known C3 wave function from [8]. The C3 wave function of Belkić [8] adapted to ionization by impact of electrons [62,63,69,70] and photons [65,66] emerged as very accurate when compared to experimental data. This is expected from the earlier documented success of the CDW-3B [8] and CDW-EIS-3B [46] methods, as reviewed in [47,48].

The CDW-3B method [8] was extensively applied to various ionizing collisions over the past three decades (see some of the most recent computations [69–75]). In these studies on differential and total cross sections for single electron emission from atoms by multiply charged ions, the CDW-3B method [8] was established as the most successful high-energy theory of ionization above 80 keV/amu. This is similar to the corresponding validity limit $E(\text{keV/amu}) \geq \max\{|E_i|, |E_f|\}$, which was assessed empirically for electron capture [7]. Here, E_i and E_f are the initial and final binding energy, respectively. Clearly, the CDW-3B theory is not applicable below its lower limit of validity, but at energies smaller than 100 keV/amu, the CDW-EIS-3B method [46] can be used to obtain total cross sections that are systematically in excellent agreement with experimental data.

The CDW-3B method can be generalized to derive the CDW-4B method for single ionization of a helium-like atomic system by a bare nucleus in a typical process of the following kind:

$$Z_P + (Z_T; e_1, e_2)_i \longrightarrow Z_P + (Z_T; e_2)_f + e_1. \tag{3.3}$$

As a prototype of this class of collisions, we shall analyze and illustrate single electron detachment from H^- by H^+:

$$H^+ + H^-(1s^2) \longrightarrow H^+ + H + e. \tag{3.4}$$

This process represents a very important example of ionizing four-body collisions where the dependence of cross sections on inter-electron correlations can be investigated. It is well-known that a strong electronic correlation effect exists in collisions involving the negative hydrogen ion H^-.

[2] The peaking approximation from [54] is of the same type as that from the previously introduced Vainstein–Presnyakov–Sobelman (VPS) approximation [57–61].

4 The MCB-4B method

Electron detachment collision (3.4) was the subject of intensive studies over three and half decades both from the theoretical and experimental viewpoints [76–92]. As to theory, use was made of the four-body plane wave Born (PWB-4B) approximation as well as the eikonal Coulomb-Born (ECB-4B) method by Gayet et al. [79], the four-body first Born (B1-4B) approximation by Bell et al. [80], the molecular orbital (MO) method by Sidis et al. [81], the atomic orbital (AO) method by Ermolaev [83], the MCB-4B method by Belkić [49,50], etc.[3] We shall primarily focus our attention upon the analysis of the PWB, B1, ECB and MCB methods, but the results of the AO and MO methods will also be presented.

The transition amplitudes in the prior versions of the ECB and MCB methods for process (3.4) are given by:[4]

$$
\begin{aligned}
T_{if}^{(\mathrm{ECB})-} &= \left\langle \chi_f^- | V_i^{(\mathrm{ECB})} | \chi_i^+ \right\rangle \\
&= \tilde{N}^{-*}(\zeta) \iiint \mathrm{d}\boldsymbol{s}_1 \mathrm{d}\boldsymbol{x}_1 \mathrm{d}\boldsymbol{x}_2 \, \mathrm{e}^{i\boldsymbol{q}\cdot\boldsymbol{s}_1 - i(\boldsymbol{\kappa}+\boldsymbol{q})\cdot\boldsymbol{x}_1} \varphi_f^*(\boldsymbol{x}_2) \\
&\quad \times {}_1F_1(i\zeta, 1, ips_1 + i\boldsymbol{p}\cdot\boldsymbol{s}_1)(vs_1 + \boldsymbol{v}\cdot\boldsymbol{s}_1)^{-i\nu_\mathrm{P}} V_i^{(\mathrm{ECB})} \varphi_i(\boldsymbol{x}_1, \boldsymbol{x}_2), \quad (4.1) \\
T_{if}^{(\mathrm{MCB})-} &= \left\langle \chi_f^- | V_i^{(\mathrm{MCB})} | \chi_i^+ \right\rangle \\
&= \tilde{N}^{-*}(\zeta) \iiint \mathrm{d}\boldsymbol{s}_1 \mathrm{d}\boldsymbol{x}_1 \mathrm{d}\boldsymbol{x}_2 \, \mathrm{e}^{i\boldsymbol{q}\cdot\boldsymbol{s}_1 - i(\boldsymbol{\kappa}+\boldsymbol{q})\cdot\boldsymbol{x}_1} \varphi_f^*(\boldsymbol{x}_2) \\
&\quad \times {}_1F_1(i\zeta, 1, ips_1 + i\boldsymbol{p}\cdot\boldsymbol{s}_1)(vs_1 + \boldsymbol{v}\cdot\boldsymbol{s}_1)^{-i\nu_\mathrm{P}} V_i^{(\mathrm{MCB})} \varphi_i(\boldsymbol{x}_1, \boldsymbol{x}_2), \quad (4.2) \\
V_i^{(\mathrm{ECB})} &= -\frac{1}{s_1} + \Delta V_{\mathrm{P}_2}, \quad (4.3) \\
V_i^{(\mathrm{MCB})} &\equiv \left(-\frac{1}{s_1} + \Delta V_{\mathrm{P}_2} \right) - \left[-\frac{1}{s_1} - u_i - \frac{\nu_\mathrm{P}}{s_1} \frac{1 + i(\boldsymbol{v}s_1 + v\boldsymbol{s}_1)\cdot\boldsymbol{\nabla}_{x_1}}{vs_1 + \boldsymbol{v}\cdot\boldsymbol{s}_1} \right] \quad (4.4) \\
&= \left[\Delta V_{\mathrm{P}_2} + u_i \right] + \frac{\nu_\mathrm{P}}{s_1} \frac{1 + i(\boldsymbol{v}s_1 + v\boldsymbol{s}_1)\cdot\boldsymbol{\nabla}_{x_1}}{vs_1 + \boldsymbol{v}\cdot\boldsymbol{s}_1}, \quad (4.5)
\end{aligned}
$$

$$
\tilde{N}^-(\zeta) = (2\pi)^{-3/2}\Gamma(1 + i\zeta)\,\mathrm{e}^{\pi\zeta/2}, \qquad \zeta = \frac{1}{p},
$$

$$
\Delta V_{\mathrm{P}_2} = \frac{1}{R} - \frac{1}{s_2}, \qquad u_i\varphi_i = (h_i - E_i)\varphi_i \equiv O_i,
$$

$$
\boldsymbol{q} = \boldsymbol{k}_f - \boldsymbol{k}_i = \boldsymbol{\eta} + \frac{E_i - E_f - E_\kappa}{v}\hat{\boldsymbol{v}}, \qquad \boldsymbol{\eta}\cdot\boldsymbol{v} = 0
$$

[3] To simplify the notation, whenever there is no chance for confusion, we will leave out part 4B (four-body) from the acronyms of the listed methods.

[4] In process (3.3), the screened inter-nuclear potential $Z_\mathrm{P}(Z_\mathrm{T}-1)/R$ is present only through the remaining eikonal phase factor $(\mu v\rho)^{2iZ_\mathrm{P}(Z_\mathrm{T}-1)/v}$. In the particular case of electron detachment (3.4), even this latter phase disappears altogether, since here $Z_\mathrm{T} = 1$.

$$E_\kappa = \frac{\kappa^2}{2}, \qquad \nu_{\rm P} = \frac{1}{v}, \qquad \boldsymbol{p} = \boldsymbol{\kappa} - \boldsymbol{v}, \tag{4.6}$$

where h_i is the target Hamiltonian. It is clear from (4.3) and (4.4) that the only difference between the ECB and MCB methods is in the perturbation potentials $V_i^{\rm (ECB)}$ and $V_i^{\rm (MCB)}$. Both methods possess the same initial χ_i^+ and final χ_f^- distorted wave functions that read as follows:

$$\chi_i^+ = \varphi_i(\boldsymbol{x}_1, \boldsymbol{x}_2) {\rm e}^{i\boldsymbol{k}_i \cdot \boldsymbol{r}_i} (v s_1 + \boldsymbol{v} \cdot \boldsymbol{s}_1)^{-i\nu_{\rm P}}, \tag{4.7}$$

$$\chi_f^- = \tilde{N}^-(\zeta) {\rm e}^{i\boldsymbol{k}_f \cdot \boldsymbol{r}_i + i\boldsymbol{\kappa} \cdot \boldsymbol{x}_1} \varphi_f(\boldsymbol{x}_2) {}_1F_1(-i\zeta, 1, -ips_1 - i\,\boldsymbol{p} \cdot \boldsymbol{s}_1). \tag{4.8}$$

Both functions (4.7) and (4.8) exhibit the correct asymptotic behaviors. By contrast, the initial perturbation in the ECB method is incorrect, since $V_i^{\rm (ECB)}$ from (4.3) is not connected to χ_i^+. On the other hand, expression (4.4) or (4.5) for $V_i^{\rm (MCB)}$ is correct. This latter potential is obtained directly and uniquely from the application of the full Schrödinger operator $H - E$ to χ_i^+, following the definition of a generic perturbation. As before, the labels H and E refer to the total Hamiltonian and energy of the entire system, respectively. The interaction $V_{\rm P_2} = -1/s_2$ between the projectile P and electron e_2 can lead to ionization of e_1 in an indirect manner through the static electronic correlations (SEC) in the target wave function. The potential $V_{\rm P2}$ is found to contribute negligibly and, therefore, this term is ignored in computations using the ECB and MCB methods. The potential operator O_i appears in $T_{if}^{\rm (MCB)-}$ from (4.2) because of the unavailability of the exact wave function φ_i of the two-electron bound state of H^-. It was shown for double capture $Z_{\rm P} + (Z_{\rm T}; 2e)_i \to (Z_{\rm P}; 2e)_f + Z_{\rm T}$ [93] and transfer ionization $Z_{\rm P} + (Z_{\rm T}; 2e)_i \to (Z_{\rm P}; e)_f + Z_{\rm T} + e$ [94] that the term O_i does not give a significant contribution. The same conclusion also holds true for single electron detachment in process (3.4). Therefore, the term O_i can be neglected in $T_{if}^{\rm (MCB)-}$, as in in the previous studies [49,50].

The integrals over $\boldsymbol{x}_1$ and $\boldsymbol{x}_2$ in (4.1) and (4.2) involve only the bound-state wave functions. This circumstance permits the use of the most elaborate wave function $\varphi_i(\boldsymbol{x}_1, \boldsymbol{x}_2)$ with any available degree of electronic correlations. To this end, we employ two classes of the best wave functions of the ground state of $H^-(^1S)$ such as the many-parameter correlated configuration interaction (CI) wave functions of Tweed [95], as well as Joachain and Terao [96]. It is illustrative to compare the results from these comprehensive computations with highly correlated wave functions in terms of some 21–61 variational parameters with the finding from the simple CI orbitals of Silverman et al. [97] with 2 and 3 variational parameters for the $(1s1s')$ and $\{(1s1s'), (2p)^2\}$ descriptions of φ_i, respectively. In these computations, the electron e_2 is viewed as being passive in the exit channel in the sense of occupying only the ground state $f = 1s$ of the target rest $H(1s)$. Under such a circumstance, each term from the prior form $T_{if}^{\rm (MCB)-}$ in (4.2) with the CI orbitals having non-zero values of the angular momentum quantum number ($l_i \neq 0$) becomes zero because of the orthogonality of the spherical harmonics through $\int {\rm d}\hat{\boldsymbol{x}}_2 Y_{0,0}(\hat{\boldsymbol{x}}_2) Y^*_{l_i m_i}(\hat{\boldsymbol{x}}_2) = \delta_{l_i,0}\delta_{m_i,0}$. However, the influence of the electronic angular correlations in $\varphi_i(\boldsymbol{x}_1, \boldsymbol{x}_2)$ is still indirectly present in (4.2), because the collection of the variational parameters alongside the binding

energy E_i possess different values for the CI orbitals with the angular momentum $l_i = 0$ and $l_i \neq 0$. The 2-parameter CI wave function of Silverman et al. [97] for the $(1s1s')$ description of the ground state ^1S of H^- reads as:

$$\begin{aligned}\varphi_i(\boldsymbol{x}_1, \boldsymbol{x}_2) &= 0.03146105 \left[\mathrm{e}^{-1.039230\, x_1 - 0.2832215\, x_2} + (x_1 \longleftrightarrow x_2)\right] \\ E_i &= -0.51330289. \end{aligned} \tag{4.9}$$

This CI orbital includes only the radial correlations via a pure s-wave. On the other hand, the 3-parameter $\{(1s1s'), (2p)^2\}$ CI wave function for $H^-(^1S)$ [97], which incorporates both radial and angular correlations (s- and p-waves) is given by:

$$\begin{aligned}\varphi_i(\boldsymbol{x}_1, \boldsymbol{x}_2) &= 0.036902815 \left[\mathrm{e}^{-1.03556\, x_1 - 0.323563\, x_2} + (x_1 \longleftrightarrow x_2)\right] \\ &\quad -0.074119614 \sum_{m_i'=-1}^{1} \varphi_{21,m_i'}(\boldsymbol{x}_1)\varphi_{21,-m_i'}(\boldsymbol{x}_2) \\ E_i &= -0.5245743, \end{aligned} \tag{4.10}$$

where $\varphi_{21,m_i'}(\boldsymbol{x}_k) = x_k\, \mathrm{e}^{-0.998504\, x_k} Y_{1,m_i'}(\hat{\boldsymbol{x}}_k)(k = 1, 2)$. Due to the orthogonality of $Y_{1,m_i'}$ with $Y_{0,0}$, all the three terms ($m_i' = 0, \pm 1$) vanish in the summation in (4.10) for the T-matrix element $T_{if}^{(\mathrm{MCB})-}$. Thus, the same algorithm used for the $(1s1s')$ configuration (4.9) can also be employed for $\{(1s1s'), (2p)^2\}$ from (4.10) by merely changing the values of the set of the variational parameters as well as E_i. Similar remarks for $l_i \neq 0$ also apply to the CI wave function of Joachain and Terao [96] which is defined by:

$$\begin{aligned}\varphi_i(\boldsymbol{x}_1, \boldsymbol{x}_2) &= \frac{1}{4\pi} \sum_{l_i'=0}^{3} \left\{ \sum_{m_i'} \sum_{m_i''} A_{m_i' m_i''}^{(l_i')} x_1^{l_i'} x_2^{l_i'} \left(x_1^{m_i'} x_2^{m_i''} + x_1^{m_i''} x_2^{m_i'} \right) \mathrm{e}^{-\lambda(x_1 + x_2)} \right\} \\ &\quad \times P_{l_i'}(\cos\theta_{12}). \end{aligned} \tag{4.11}$$

The two-electron CI orbitals obtained by Tweed [95] are of the same form (4.11) except for the redefinition $x_1^{l_i'} x_2^{l_i'} \equiv 1$. In (4.11), the function $P_{l_i'}(\cos\theta_{12})$ is the Legendre polynomial, whereas the coefficients $A_{m_i' m_i''}^{(l_i')}$ are the linear variational parameters and $\theta_{12} = \cos^{-1}\left(\hat{\boldsymbol{x}}_1 \cdot \hat{\boldsymbol{x}}_2\right)$. The pure s-waves $P_0(\cos\theta_{12})$ are the only ones that need to be explicitly retained in (4.11) for the analytical calculation of $T_{if}^{(\mathrm{MCB})-}$. However, the remaining terms with $P_{l_i' \neq 0}(\cos\theta_{12})$ are implicitly present in the final results through influencing the numerical values of the linear $\left\{A_{m_i' m_i''}^{(l_i')}\right\}$ and non-linear (λ) coefficients, as well as the binding energy E_i determined by the standard Rayleigh–Ritz variational principle. Using the 61-parameter CI wave function (4.11) from [96], the binding energy $E_i = -0.5272225$ is obtained. The associated 'exact' value $E_i = -0.527751016544203$ is available from the Hylleraas r_{12}-dependent

wave function containing some formidable 616 variational parameters, as used by Drake [98].

The dynamic correlations are absent from the prior transition amplitude $T_{if}^{(\mathrm{MCB})-}$ in (4.2) because the electron-electron repulsion $V_{12} = 1/x_{12} \equiv 1/|\boldsymbol{x}_1 - \boldsymbol{x}_2|$ does not appear in the perturbation $V_i^{(\mathrm{MCB})}$, which produces the transition in process (3.4). Potential V_{12} could be present in $T_{if}^{(\mathrm{MCB})-}$ by retaining the small eigenvalue correction O_i for an approximate wave function φ_i. This is clear from $O_i = (h_i - E_i)\varphi_i = (E_i + \nabla_1^2/2 + \nabla_2^2/2 + 1/x_1 + 1/x_2 - 1/x_{12})\varphi_i \neq 0$. However, such an appearance of V_{12} in $V_i^{(\mathrm{MCB})}$ is still linked to the static correlation, because O_i which leads to $1/x_{12}$ stems from a non-exact structural description of the target H^- and not from any collisional dynamics.

The true dynamic correlations due to the dielectronic interaction in the course of the collision in process (3.4) are explicitly present in the post form of the transition amplitude $T_{if}^{(\mathrm{MCB})+}$:

$$
\begin{aligned}
T_{if}^{(\mathrm{MCB})+} &= \left\langle \chi_f^- | V_f^{(\mathrm{MCB})} | \chi_i^+ \right\rangle \\
&= \tilde{N}^{-*}(\zeta) \iiint \mathrm{d}\boldsymbol{s}_1 \mathrm{d}\boldsymbol{x}_1 \mathrm{d}\boldsymbol{x}_2 \mathrm{e}^{i\boldsymbol{q}\cdot\boldsymbol{s}_1 - i(\boldsymbol{\kappa}+\boldsymbol{q})\cdot\boldsymbol{x}_1} \varphi_f^*(\boldsymbol{x}_2) \\
&\quad \times {}_1F_1(i\zeta, 1, ips_1 + i\boldsymbol{p}\cdot\boldsymbol{s}_1)(vs_1 + \boldsymbol{v}\cdot\boldsymbol{s}_1)^{-i\nu_\mathrm{P}} V_f^{(\mathrm{MCB})} \varphi_i(\boldsymbol{x}_1, \boldsymbol{x}_2), \quad (4.12) \\
V_f^{(\mathrm{MCB})} &= \Delta V_{12} + \Delta V_{\mathrm{P}_2}, \quad (4.13) \\
\Delta V_{12} &= \frac{1}{x_{12}} - \frac{1}{x_1}, \qquad \Delta V_{\mathrm{P}_2} = \frac{1}{R} - \frac{1}{s_2}. \quad (4.14)
\end{aligned}
$$

The static correlations are contained in the post matrix element $T_{if}^{(\mathrm{MCB})+}$ via φ_i and ΔV_{P_2}. As discussed, ΔV_{P_2} can be neglected, because it plays an insignificant role in process (3.4). As a consequence, the integrals $\int \mathrm{d}\boldsymbol{s}_1(\cdots)$ and $\int\int \mathrm{d}\boldsymbol{x}_1 d\boldsymbol{x}_2(\cdots)$ in (4.1), (4.2) and (4.12) become independent of each other. These integrals over $\boldsymbol{x}_1, \boldsymbol{x}_2$ and $\boldsymbol{s}_1$ can be calculated analytically by using e.g. the pertinent real integral representation from [99] for the functions $(vs_1 + \boldsymbol{v}\cdot\boldsymbol{s}_1)^{-i\nu_\mathrm{P}}$ and $(vs_1 + \boldsymbol{v}\cdot\boldsymbol{s}_1)^{-i\nu_\mathrm{P}-1}$.

The T-matrix element between any fixed initial χ_i^+ and final χ_f^- on-shell distorted waves can be introduced by $T_{if} = \langle \chi_f^- | H - E | \chi_i^+ \rangle$. Here, the operator $H - E$ can be applied to either χ_i^+ or χ_f^-. When the wave function to which the operator $H - E$ acts is the exact on-shell scattering state, a zero state vector $\emptyset$ is obtained. Whenever the initial or final bound state wave function is not exact, the ensuing T-matrix elements $T_{if}^- = \langle \chi_f^- | \xi_i^+ \rangle$ and $T_{if}^+ = \langle \xi_f^- | \chi_i^+ \rangle$ with $\xi_i^+ \equiv (H - E)\chi_i^+ \neq \emptyset$ and $\xi_f^- \equiv (H - E)\chi_f^- \neq \emptyset$ differ from each other, $T_{if}^- \neq T_{if}^+$. This occurs in the entrance channel of process (3.4) leading to the post-prior discrepancy in every particular method. To estimate this discrepancy in the MCB theory, we shall analyze the results for the total cross sections obtained by using the prior (4.2) and post (4.12) forms of the transition amplitude.

In addition to the ECB method, Gayet et al. [79] employed the PWB approximation. In this latter approximation, the relative motions of the heavy nuclei in the entrance

and exit channel are described by the plane waves. Moreover, the plane wave is used for the emitted electron in the final state. Obviously, the PWB approximation does not obey the correct boundary conditions for the initial and final scattering states in process (3.4). The transition amplitude $T_{if}^{(\mathrm{PWB})-}$ in the PWB approximation can be obtained by putting $\nu_{\mathrm{P}} = 0 = \zeta$ in the expression (4.1) from the ECB method:

$$T_{if}^{(\mathrm{PWB})-} = (2\pi)^{-3/2} \iiint \mathrm{d}\boldsymbol{x}_1 \mathrm{d}\boldsymbol{x}_2 \mathrm{d}\boldsymbol{R}\, \mathrm{e}^{i\boldsymbol{q}\cdot\boldsymbol{s}_1 - i(\boldsymbol{\kappa}+\boldsymbol{q})\cdot\boldsymbol{x}_1} \varphi_f^*(\boldsymbol{x}_2) \times \left(\frac{1}{R} - \frac{1}{s_1} - \frac{1}{s_2}\right) \varphi_i(\boldsymbol{x}_1, \boldsymbol{x}_2). \tag{4.15}$$

Both ν_{P} and ζ tend to zero as $E \to \infty$. Therefore, at asymptotically high impact energies, it follows $Q_{if}^{(\mathrm{ECB})-} \longrightarrow Q_{if}^{(\mathrm{PWB})-}$:

$$Q_{if}^{(\mathrm{ECB})-} \approx Q_{if}^{(\mathrm{PWB})-} \qquad (v \gg 1). \tag{4.16}$$

In the work of Gayet et al. [79], the 2-parameter CI wave function (4.9) of Silverman et al. [97] was employed for the initial state $\varphi_i(\boldsymbol{x}_1, \boldsymbol{x}_2)$. This discrete wave function is not orthogonal to the plane wave final state:

$$\varphi_f(\boldsymbol{x}_1, \boldsymbol{x}_2) = \phi_{\boldsymbol{\kappa}}(\boldsymbol{x}_1)\varphi_f(\boldsymbol{x}_2), \qquad \phi_{\boldsymbol{\kappa}}(\boldsymbol{x}_1) = (2\pi)^{-3/2}\mathrm{e}^{-i\boldsymbol{\kappa}\cdot\boldsymbol{x}_1}, \quad \langle\varphi_f|\varphi_i\rangle \neq 0. \tag{4.17}$$

Under this circumstance, integration over $\boldsymbol{R}$ reduces (4.15) to the expression:

$$T_{if}^{(\mathrm{PWB})-} = \frac{2}{q^2}(2\pi)^{-1/2} \int\int \mathrm{d}\boldsymbol{x}_1 \mathrm{d}\boldsymbol{x}_2\, \varphi_f^*(\boldsymbol{x}_2) \times \left(1 - \mathrm{e}^{-i\boldsymbol{q}\cdot\boldsymbol{x}_1} - \mathrm{e}^{-i\boldsymbol{q}\cdot\boldsymbol{x}_2}\right) \varphi_i(\boldsymbol{x}_1, \boldsymbol{x}_2). \tag{4.18}$$

This matrix element can further be calculated analytically giving a simple closed formula for $T_{if}^{(\mathrm{PWB})-}$. The meaning of the expression (4.18) becomes clear in the high energy limit by using the Maclaurin expansion of both exponentials $\exp(-i\boldsymbol{q}\cdot\boldsymbol{x}_k)(k = 1, 2)$ and retaining only the first two terms. In this way, the term $1 - \sum_{k=1}^{2} \exp(-i\boldsymbol{q}\cdot\boldsymbol{x}_k)$ in (4.18) is simplified via $1 - \sum_{k=1}^{2} \exp(-i\boldsymbol{q}\cdot\boldsymbol{x}_k) \approx -1 + i\boldsymbol{q}\cdot(\boldsymbol{x}_1 + \boldsymbol{x}_2)$. Therefore, the asymptotic behavior of the transition amplitude in the PWB approximation becomes:

$$T_{if}^{(\mathrm{PWB})-} \approx \tilde{T}_{if}^{(\mathrm{PWB})-} \approx \frac{2}{q^2}(2\pi)^{-1/2} \int\int \mathrm{d}\boldsymbol{x}_1 \mathrm{d}\boldsymbol{x}_2 \varphi_f^*(\boldsymbol{x}_2) \times \left[-1 + i\boldsymbol{q}\cdot(\boldsymbol{x}_1 + \boldsymbol{x}_2)\right] \varphi_i(\boldsymbol{x}_1, \boldsymbol{x}_2) \qquad (v \gg 1). \tag{4.19}$$

This result implies that at sufficiently high impact energies, the total cross sections $Q_{if}^{(\mathrm{PWB})-}$ and $\tilde{Q}_{if}^{(\mathrm{PWB})-}$ from (4.15) and (4.19), respectively, shall equalize:

$$Q_{if}^{(\mathrm{PWB})-} \approx \tilde{Q}_{if}^{(\mathrm{PWB})-} \qquad (v \gg 1). \tag{4.20}$$

This procedure for arriving at the asymptotic limit of total cross sections for ionization is similar to the dipole-type approximation. It is well-known that the dipole approximation for ionization must yield the high-energy limit $Q_{if} \propto (1/E)\ln(E)$, because this formula follows exclusively from the dipole term $i\boldsymbol{q}\cdot(\boldsymbol{x}_1+\boldsymbol{x}_2)$. The cross section $\tilde{Q}_{if}^{(\mathrm{PWB})-}$ possesses the function $i\boldsymbol{q}\cdot(\boldsymbol{x}_1+\boldsymbol{x}_2)-1$ as seen in (4.19), where the second term (unity) dominates over the dipole contribution at high energies. Because of this non-zero contribution from the mentioned constant term, the cross sections $\tilde{Q}_{if}^{(\mathrm{PWB})-}$ and $Q_{if}^{(\mathrm{PWB})-}$ do not exhibit the obligatory high-energy asymptote $Q_{if} \propto (1/E)\ln(E)$. Precisely the same drawback is encountered in $Q_{if}^{(\mathrm{ECB})-}$ as per (4.16). The explicit computations by Gayet et al. [79] confirm this expectation.

When the initial $\varphi_i(\boldsymbol{x}_1,\boldsymbol{x}_2)$ and final $\varphi_f(\boldsymbol{x}_1,\boldsymbol{x}_2)$ states of the H^- ion are orthogonal, the contribution from the unit term is equal to zero. If these states are non-orthogonal, it is easy to orthogonalize them by means of the Gramm-Schmidt procedure. This is readily accomplished by constructing the final state $\varphi_f(\boldsymbol{x}_1,\boldsymbol{x}_2)$ of the H^- ion via:

$$\begin{aligned}
\varphi_f(\boldsymbol{x}_1,\boldsymbol{x}_2) &= \Upsilon_f(\boldsymbol{x}_1,\boldsymbol{x}_2) - \langle\varphi_i|\Upsilon_f\rangle\varphi_i(\boldsymbol{x}_1,\boldsymbol{x}_2),\\
\Upsilon_f(\boldsymbol{x}_1,\boldsymbol{x}_2) &= \frac{1}{2}\left[\phi_{\boldsymbol{\kappa}}(\boldsymbol{x}_1)\varphi_f(\boldsymbol{x}_2)+\phi_{\boldsymbol{\kappa}}(\boldsymbol{x}_2)\varphi_f(\boldsymbol{x}_1)\right],\\
\langle\varphi_f|\varphi_i\rangle &= 0.
\end{aligned} \tag{4.21}$$

It is seen from (4.3) and (4.15) that the ECB and PWB methods possess the same perturbation potential $V_i^{(\mathrm{PWB})} \equiv 1/R - 1/s_1 - 1/s_2 = V_i^{(\mathrm{ECB})}$. When the scattering aggregates are far apart from each other, as in the asymptotic region, we can use the approximation $R \approx s_2$. This implies that $\Delta V_{\mathrm{P}_2} \approx 0$ and, hence, $V_i^{(\mathrm{PWB})} = V_i^{(\mathrm{ECB})} \approx -1/s_1$. Thus, in the asymptotic scattering region where the measurement is made, the common perturbation potential in the ECB and PMB methods is the Coulomb potential between the projectile proton and the emitted electron $(-1/s_1)$. Such an occurrence invalidates the concept of the asymptotic freedom and, therefore, the asymptotic convergence problem of Dollard [100] is ignored. This occurs because no wave packet in a Coulomb field can be attributed to free particles, since a Coulomb or Coulomb-like potential always distorts the unperturbed plane wave, even at asymptotically large inter-particle distances. Recall that the notion of free particles in the asymptotic scattering region (the region of measurement of collisional observables such as cross sections) is mandatory to ensure that one can distinguish the situation "before" and "after" collision. The situation "before collision" relates to the stage of experimental preparation of the initial state of the target in the entrance channel with the projectile beam being turned off. Likewise, the situation "after collision" corresponds to the measurement of configurations in the exit channel when the scattering is completed i.e. when all the interactions among the particles have ceased to exist.

Neither the ECB nor PWB method obeys the concept of asymptotic freedom. Therefore, it is important to assess the severity of this failure by examining the overall performance of these two models.

The standard B1 approximation is obtained by treating the entrance channel in process (3.4) in the same way as in the PWB model, and describing the single continuum state of the H^- ion in the exit channel by the Coulomb wave function for the ejected electron. This procedure has been used by Bell et al. [80] within the prior version of the B1 method for process (3.4). They employed a wave function of the final state of the H^- ion as a symmetrized function relative to the electronic coordinates $\boldsymbol{x}_1$ and $\boldsymbol{x}_2$. Their final state wave function was orthogonal to $\varphi_i(\boldsymbol{x}_1, \boldsymbol{x}_2)$ as per construction via the Gramm–Schmidt orthogonalization of the type (4.21). Nevertheless, due to the use of a plane wave for the relative inter-aggregate motion of two charged particles H^+ and H^- in the entrance channel, the B1 approximation violates the correct boundary conditions and, therefore, it is theoretically unsound.

It would also be very important to consider process (3.4) by using the CDW-4B method, as the extension of the CDW-3B method of Belkić [8]. Such an extension yields the following prior and post transition amplitudes for process (3.4) [49]:

$$\begin{aligned} T_{if}^{(\mathrm{CDW})-} = {} & \tilde{N}^{-*}(\zeta) N^{+}(\nu_\mathrm{P}) \iiint \mathrm{d}\boldsymbol{s}_1 \mathrm{d}\boldsymbol{x}_1 \mathrm{d}\boldsymbol{x}_2 \mathrm{e}^{i\boldsymbol{q}\cdot\boldsymbol{s}_1 - i(\boldsymbol{\kappa}+\boldsymbol{q})\cdot\boldsymbol{x}_1} \varphi_f^*(\boldsymbol{x}_2) \\ & \times {}_1F_1(i\zeta, 1, ips_1 + i\boldsymbol{p}\cdot\boldsymbol{s}_1) \left[\left(\Delta V_{\mathrm{P}_2} + O_i\right) \varphi_i(\boldsymbol{x}_1, \boldsymbol{x}_2) \right. \\ & \times {}_1F_1(i\nu_\mathrm{P}, 1, ivs_1 + i\boldsymbol{v}\cdot\boldsymbol{s}_1) \\ & \left. - \boldsymbol{\nabla}_{s_1} {}_1F_1(i\nu_\mathrm{P}, 1, ivs_1 + i\boldsymbol{v}\cdot\boldsymbol{s}_1) \cdot \boldsymbol{\nabla}_{x_1} \varphi_i(\boldsymbol{x}_1, \boldsymbol{x}_2) \right], \end{aligned} \tag{4.22}$$

$$\begin{aligned} T_{if}^{(\mathrm{CDW})+} = {} & \tilde{N}^{-*}(\zeta) N^{+}(\nu_\mathrm{P}) \iiint \mathrm{d}\boldsymbol{s}_1 \mathrm{d}\boldsymbol{x}_1 \mathrm{d}\boldsymbol{x}_2 \, \mathrm{e}^{i\boldsymbol{q}\cdot\boldsymbol{s}_1 - i(\boldsymbol{\kappa}+\boldsymbol{q})\cdot\boldsymbol{x}_1} \varphi_f^*(\boldsymbol{x}_2) \\ & \times {}_1F_1(i\zeta, 1, ips_1 + i\boldsymbol{p}\cdot\boldsymbol{s}_1) \left(\Delta V_{\mathrm{P}_2} + \Delta V_{12}\right) \varphi_i(\boldsymbol{x}_1, \boldsymbol{x}_2) \\ & \times {}_1F_1(i\nu_\mathrm{P}, 1, ivs_1 + i\boldsymbol{v}\cdot\boldsymbol{s}_1), \end{aligned} \tag{4.23}$$

where $N^+(\nu_\mathrm{P}) = \Gamma(1 - i\nu_\mathrm{P})\, \mathrm{e}^{\pi\nu_\mathrm{P}/2}$ and $\nu_\mathrm{P} = 1/v$. It is also possible to further approximate $T_{if}^{(\mathrm{CDW})+}$ to obtain the CDW-EIS model as was done by Crothers and McCann [46]. This was achieved through the replacement of the wave function $N^+(\nu_\mathrm{P})\,{}_1F_1(i\nu_\mathrm{P}, 1, ivs_1 + \boldsymbol{v}\cdot\boldsymbol{s}_1)$ from the CDW method by the associated asymptotic form $(vs_1 + \boldsymbol{v}\cdot\boldsymbol{s}_1)^{-i\nu_\mathrm{P}}$, which is valid only for $|vs_1 + \boldsymbol{v}\cdot\boldsymbol{s}_1| \gg 1$. In this way, in the case of process (3.4), the resulting T-matrix element $T_{if}^{(\mathrm{CDW-EIS})}$ is formally the same as the transition amplitude $T_{if}^{(\mathrm{MCB})+}$ from (4.12). However, as opposed to the simplifying derivation of Crothers and McCann [46], the MCB method in either its prior or post form from (4.2) or (4.12) was autonomously derived by Belkić [49,50] for process (3.4) without any reliance upon the CDW approximation.

Once the transition amplitudes are available, the triple differential $\mathrm{d}^3 Q_{if}^{\pm}/\mathrm{d}\boldsymbol{\kappa}$ and total $Q_{if}^{\pm}$ cross sections for process (3.4) can, respectively, be introduced as:

$$\frac{\mathrm{d}^3 Q_{if}^{\pm}}{\mathrm{d}\boldsymbol{\kappa}} = \int \mathrm{d}\boldsymbol{\eta} \left| \frac{T_{if}^{\pm}(\boldsymbol{\eta})}{2\pi v} \right|^2, \tag{4.24}$$

$$Q_{if}^{\pm} = \int \mathrm{d}\kappa \, \frac{\mathrm{d}^3 Q_{if}^{\pm}}{\mathrm{d}\kappa}. \tag{4.25}$$

In the non-relativistic spin-independent formalism, as the one used for processes (3.3) and (3.4), the final results for $\mathrm{d}^3 Q_{if}^{\pm}/\mathrm{d}\kappa$ and $Q_{if}^{\pm}$ must be multiplied by a factor of 2 because either of the electrons e_1 or e_2 can detached from the target H^- with equal probability.

5 Comparison between theories and experiments

Throughout this Section, we shall limit our analysis to the ground state of the atomic hydrogen H($1s$) in the exit channel of process (3.4). However, the measurements for electron detachment from [87–89] and [101] correspond to all bound and continuous states of the target remainder H. Thus, for a fuller comparison of theory and experiment, a new computation is needed including the whole discrete and continuous spectrum of atomic hydrogen. Simultaneous detachment and excitation (or detachment and ionization) in process (3.4) are interesting and important to investigate [5]. However, it is expected that for process (3.4), probabilities for these two-electron processes are small with respect to single electron detachment leaving the target rest in the ground state, H($1s$). Under such a circumstance, it is justified to confront the experimental data for process (3.4) with the theoretical cross sections for a simpler reaction:

$$H^+ + H^-(1s^2) \longrightarrow H^+ + H(1s) + e. \tag{5.1}$$

In Fig. 1, it is seen that the total cross sections $Q_{if}^{(\mathrm{ECB})-}$ for process (5.1), obtained by Gayet et al. [79] with the 2-parameter radially correlated CI wave function of Silverman et al. [97] for $H^-(1s^2)$ flagrantly overestimate the experimental data by 2–3 orders of magnitude. Additionally, the prediction $Q_{if}^{(\mathrm{ECB})-}$ in the ECB model from [79] tends to a constant for large values of the impact energy E, in sharp contrast with the correct Bethe asymptotic limit, $Q_{if} \propto (1/E)\ln(E)$. These astonishing failures of the ECB method could have been noticed by reference to the earlier work of Peart et al. [87] who published the related experimental data with electrons as projectiles. Of course, close agreement is known to exist between total cross sections for fast electron and proton impact ionization or detachment processes at the equivalent or scaled energies (or the same impact velocities). In Fig. 1, we plot only the measurement from [87], since these experimental data were available at the time of the appearance of the results of Gayet et al. [79]. Likewise, Gayet et al. [79] could have employed the scaled cross sections of the Coulomb-Born (CB) method from the investigation of Belly and Schwartz [78] for $e - H^-$ detachment with the obtained proper Bethe asymptote to observe that the ECB method is utterly unphysical. Clearly, the very first indication that something was unphysical in the computations from [79] was a plateau in the cross sections $Q_{if}^{(\mathrm{ECB})-}$ reached at high energies, as shown in Fig. 1, instead of attaining the required Bethe asymptotic behavior $Q_{if} \propto (1/E)\ln(E)$. Moreover, being presumably unaware of the experimental data from [87], the work of Gayet et al. [79] was further misguided by their own results from the PWB approximation. The

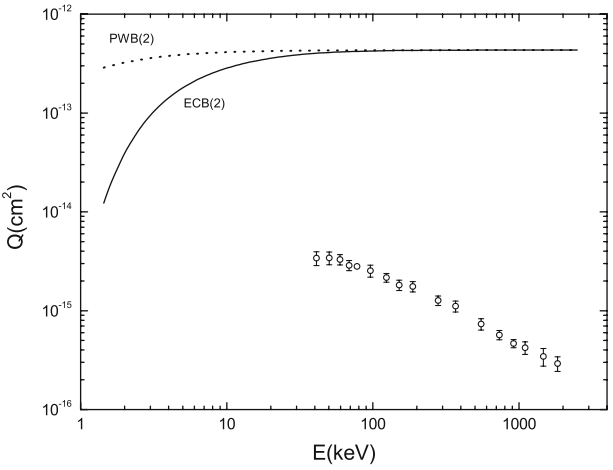

Fig. 1 Total cross sections Q as a function of the incident energy E for process (3.4). Theory: *full curve* (ECB method [79]) and *dotted curve* (PWB method [79]). Integer 2 with the acronyms is the number of variational parameters in the target CI wave function of Silverman et al. [97]. Experiment: *circle* [87]. The original data of Peart et al. [87] are for electron impact, and here they are scaled to the equivalent proton impact energy

PWB model is seen in Fig. 1 to give the erroneous cross sections $Q_{if}^{(\mathrm{PWB})-}$ that at high energies also tend to precisely the same peculiar constant predicted by the ECB method.

Recall that a previous study of Geltman [76] within the plane wave Born–Oppenheimer (PWBO) approximation on detachment in the $e - \mathrm{H}^-$ collisions yielded the total cross sections that tend to a constant value at high impact energies, at variance with the Bethe asymptotic limit $Q_{if} \propto (1/E)\ln(E)$. This is reminiscent of the situation with the ECB method in Fig. 1. In a subsequent investigation, McDowell and Williamson [77] attempted to attribute this unphysical result of Geltman [76] exclusively to the lack of orthogonality between the initial and final states of the H^- ion. They claimed that, due to non-orthogonality of these latter states, the standard dipole approximation breaks down. Such a breakdown was said in [77] to occur because the constant, unity term in the series expansion of the exponential function $\exp(i\boldsymbol{q}\cdot\boldsymbol{r}) \approx 1 + i\boldsymbol{q}\cdot\boldsymbol{r}$ provides the dominant high-energy contribution compared to the dipole term $(i\boldsymbol{q}\cdot\boldsymbol{r})$. As discussed, the high-energy asymptote $Q_{if} \propto (1/E)\ln(E)$, which is the Bethe limit of total cross sections for ionization treated in the first Born approximation, stems solely from the dipole term. The argument of McDowell and Williamson [77] on the spurious contribution of the said constant term in a series expansion of the exponential should be revisited. These authors were wrong when concluding that the initial and final states of H^- must necessarily be orthogonal in order to eliminate this spurious contribution. Their conclusion misled several subsequent studies that systematically tried to impose orthogonality of the initial and final states in various methods. Naturally, it is appropriate to construct the initial (bound) and (final) continuum states of the H^- ion in such a way that they are orthogonal to each other. Nevertheless, scattering theory does not require orthogonality between the scattering wave functions of the whole entrance

and exit channel (nor of the unperturbed initial and final states). Rather the opposite is true, since formal scattering theory permits non-orthogonality of the eigen-vectors of two different channel Hamiltonians $H_i \neq H_f$ for $i \neq f$ (see Sect. 2 in [7]). Stated differently, the initial and final states can be uniquely defined without any reference to their orthogonality.

Therefore, while McDowell and Williamson [77] were correct in questioning the contribution of the non-dipole (constant) term, they were wrong in drawing inferences on the necessity of imposing orthogonality of the initial and final states. Moreover, we do not need to use the additional dipole approximation to any given method for ionization to arrive at the high-energy Bethe limit. Such a high-energy limit should be automatically obtained by imposing the correct boundary conditions to the entrance and exit channels. The ECB method fails to satisfy this latter requirement in the entrance channel due to the incorrect perturbation potential. As a result, $Q_{if}^{(\mathrm{ECB})-}$ levels out at high energies, rather than attaining the Bethe limit. However, this has nothing to do with non-orthogonality of the initial and final states. As stated, the dipole-type approximation to $T_{if}^{(\mathrm{ECB})-}$ at high energies demonstrates that the unit term dominates over the dipole contribution in the mentioned exponential function, precisely as was the case in McDowell and Williamson's [77] analysis of Geltman's work [76]. The reason for such an occurrence is not exclusively in the lack of orthogonality between the initial and final states H^-. This conjecture would be proven if one could obtain the proper Bethe limit for total cross sections by employing the same non-orthogonal initial and final wave functions of H^- as those used in the ECB method. Such a possibility has been indeed demonstrated in MCB method [49,50] in which $Q_{if}^{(\mathrm{MCB})-}$ was found to exhibit the correct Bethe limit.

Although the MCB and ECB theories possess the joint initial and final states, it is only the former method which has the correct perturbation potential $V_i^{(\mathrm{MCB})}$ in the prior transition amplitude $T_{if}^{(\mathrm{MCB})-}$. Specifically and by definition, $V_i^{(\mathrm{MCB})}$ from (4.4) is given by the difference $V_i^{(\mathrm{ECB})} - \Delta V_i$ in which ΔV_i reads as $\Delta V_i = V_i^{(\mathrm{ECB})} - \Delta V_i'$ where $\Delta V_i'$ is the rhs of (4.5). Imposing the proper boundary conditions in the entrance channel to the initial state χ_i^+ also requires the establishment of the correct connection between χ_i^+ and the associated perturbation potential, which produces the transition in $T_{if}^{(\mathrm{MCB})-}$. In this way, the term $V_i^{(\mathrm{ECB})}$ is canceled out in $V_i^{(\mathrm{MCB})}$ and this leads to the perturbation $V_i^{(\mathrm{MCB})} = V_i^{(\mathrm{ECB})} - [V_i^{(\mathrm{ECB})} - \Delta V_i'] = \Delta V_i'$ which, in turn, gives the Bethe limit of the high-energy cross sections $Q_{if}^{(\mathrm{MCB})-}$. Furthermore, in the dipole approximation to $T_{if}^{(\mathrm{MCB})-}$, the constant unit term from the expansion of the exponential function cancels out and this also secures the dominance of the dipole term, so that again the Bethe limit for $Q_{if}^{(\mathrm{MCB})-}$ would be obtained if the partial wave analysis is used in the MCB method. Of course, in practical calculations there is no need to resort to the partial wave representation of the MCB method. This is because the closed, analytical results for the transition amplitude $T_{if}^{(\mathrm{MCB})-}$ in this theory can advantageously be obtained without recourse to partial waves.

The main reason for the basic inadequacy of the ECB model of Gayet et al. [79] was found by Belkić [49,50]. This was done by employing the same 2-parameter wave

function of Silverman et al. [97] as in the work of Gayet et al. [79]. The said reason was in the neglect of the exact boundary conditions in the ECB method despite using the initial and final scattering wave functions with the correct asymptotic behaviors. As mentioned, the initial scattering wave function χ_i^+ in the ECB method is not linked to the corresponding perturbation potential $V_i^{(\mathrm{ECB})}$. It should be re-emphasized that the proper boundary conditions are fulfilled only when both the initial and final scattering wave functions possess the correct asymptotic behaviors and, simultaneously, if these wave functions are consistently related to the associated perturbation potentials in the entrance and exit channel, respectively.

The explanation by Belkić [49,50] for the major problem in the ECB model [79] gave also the key to the solution of this problem. In order to achieve this goal, it was sufficient to establish consistency between the initial scattering wave function and the corresponding perturbation interaction in the entrance channel. As stated earlier, the sought consistency automatically follows from the application of the Schrödinger operator $H - E$ to the initial scattering wave function χ_i^+ from the ECB model. The resulting correct perturbation interaction $V_i^{(\mathrm{MCB})}$ is substantially different from $V_i^{(\mathrm{ECB})}$. Such a modification of the perturbation potential in the entrance channel, in fact, defines the MCB method [49,50]. The final scattering wave function χ_f^- and the associated exit channel perturbation potential in the ECB model are correct, and they are consistently connected with each other. Hence there is no need to change the description of the exit channel in the ECB method when going to the MCB method. Overall, the only difference between the prior transition amplitudes $T_{if}^{(\mathrm{ECB})-}$ and $T_{if}^{(\mathrm{MCB})-}$ from (4.1) and (4.2) in the ECB and MCB methods is in their perturbation interactions $V_i^{(\mathrm{ECB})}$ and $V_i^{(\mathrm{MCB})}$ from (4.3) and (4.5), respectively.

As demonstrated by Belkić [1,2], the mentioned basic failure of the ECB method is not possible to overcome through the electronic angular correlations in the target CI wave function by including more terms with a larger number ($N = 3 - 61$) of variational parameters. This can also be seen in Figs. 2 and 3. It is evident from these two figures that despite including a high degree of static correlations, the saturation of the high-energy cross sections $Q_{if}^{(\mathrm{ECB})-}$ to certain peculiar constant values still persists in a systematic way. Further, the plateaus of $Q_{if}^{(\mathrm{ECB})-}$ are altered by using different numbers of the variational parameters in the CI wave functions of the H^- target. These computations employ three different sets of the CI ground-state wave functions $\varphi_i(\boldsymbol{x}_1, \boldsymbol{x}_2)$ for the $H^-(^1S)$. The only difference is in the number of variationally determined parameters. The simplest are 2- and 3-parameter orbitals of Silverman et al. [97]. More elaborated are the 21–41 parameter orbitals of Tweed [95], as well as the 61-parameter orbital of Joachain and Terao [96]. The conclusion from these computations illustrated in Figs. 2 and 3 shows that no appreciable improvement is gained in the ECB model even when the highly-correlated 21–61 CI wave functions are used, since the resulting cross sections $Q_{if}^{(\mathrm{ECB})-}$ still overestimate the experimental data by 2–3 orders of magnitude. Such a drastic failure was already present in the work of Gayet et al. [79] who used the simple 2-parameter CI orbital from [97] (see the

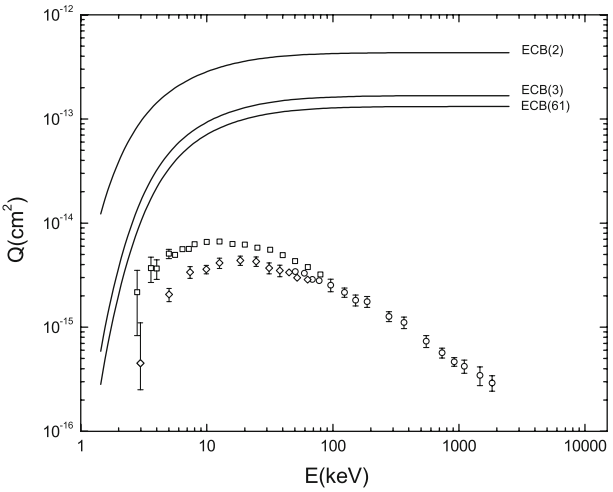

Fig. 2 Total cross sections Q as a function of the incident energy E for process (3.4). Theory: *full curves* (ECB method [79]). Integer N with the acronyms is the number of variational parameters in the target CI wave function from Silverman et al. [97] ($N = 2, 3$), as well as from Joachain and Terao [96] ($N = 61$). Experiment: *circle* [87], *diamond* [89] and *square* [101]

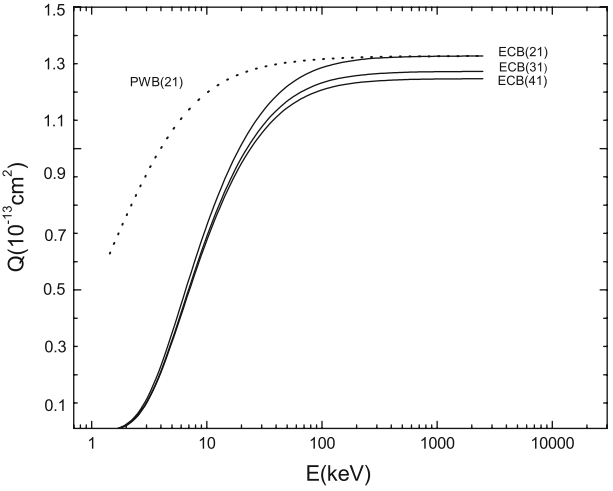

Fig. 3 Total cross sections Q as a function of the incident energy E for process (3.4). Theory: *full curves* (ECB method [79]) and *dotted curve* (PWB method [79]). Integer N with the acronyms is the number of variational parameters in the target CI wave function from Tweed [95] ($N = 21, 31, 41$)

present Fig. 1). A similar fundamental deficiency also persists in the PWB method, as seen in Fig. 3 for $N = 21$ with the like pattern for $N = 31 - 61$ (not shown).

Regarding the measurements, Fig. 2 displays other experimental data in addition to those of Peart et al. [87]. In particular, the experimental data of Peart et al. [89] and Melchert et al. [101] shown in this figure are measured with proton impact as in process (3.4), so that no conversion is needed. It is seen that at higher energies, these

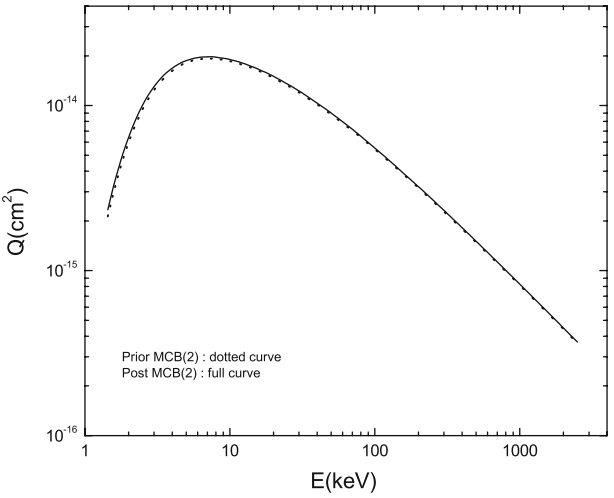

Fig. 4 Total cross sections Q as a function of the incident energy E for process (3.4). Theory: *full curve* (prior MCB method [49,50]) and *dotted curve* (post MCB method [49,50]). Integer 2 with the acronyms is the number of variational parameters in the target CI wave function from Silverman et al. [97]

two latter sets of proton impact data [89,101] merge smoothly into the associated electron impact data [87] after the appropriate scaling to the equivalent proton energies, as anticipated. Notice that the error bars at intermediate and high energies on all the experimental data depicted on Fig. 2 are relatively small. However, significantly larger uncertainties in the measurements from [89] and [101] are seen at lower energies.

Prior to making a direct comparison between the results of the ECB and MCB methods, we shall first analyze the latter theory by examining the post-prior discrepancy in Fig. 4, as well as the convergence properties with an increasing degree of static inter-electron correlations. This is illustrated in Figs. 5 and 6. In Fig. 4, a comparison is made using the cross sections in the prior Q_{if}^{-} and post Q_{if}^{+} forms from the MCB method for process (5.1) by relying upon the 2-parameter CI wave function of Silverman et al. [97]. Of primary importance to note here is a proper decline of the cross sections as the impact energy E is augmented. This is in striking contrast to the plateau in the ECB method from Fig. 1.

It can be checked that this decline of $Q_{if}^{(\mathrm{MCB})\pm}$ closely follows the Bethe asymptotic limit $\propto (1/E)\ln(E)$ at large values of E. Moreover, it is clear from Fig. 4 that excellent agreement exists between the prior $Q_{if}^{(\mathrm{MCB})-}$ and post $Q_{if}^{(\mathrm{MCB})+}$ total cross sections at all impact energies. This is a very attractive property of the MCB method despite the existing post-prior asymmetry of the perturbation potentials $V_i^{(\mathrm{MCB})}$ and $V_f^{(\mathrm{MCB})}$ from (4.5) and (4.13) in the transition amplitudes $T_{if}^{(\mathrm{MCB})-}$ and $T_{if}^{(\mathrm{MCB})+}$ given by the matrix elements (4.2) and (4.12), respectively. Therefore, a small post-prior discrepancy in Fig. 4 justifies that only one version of the MCB method can be used in detailed computations with more elaborated wave functions of H^-. Moreover, in the matrix element $T_{if}^{(\mathrm{MCB})-}$ we can ignore the small perturbations ΔV_{P_2} and O_i that do not contain the inter-electron potential $1/x_{12}$ in the role of dynamic correlations.

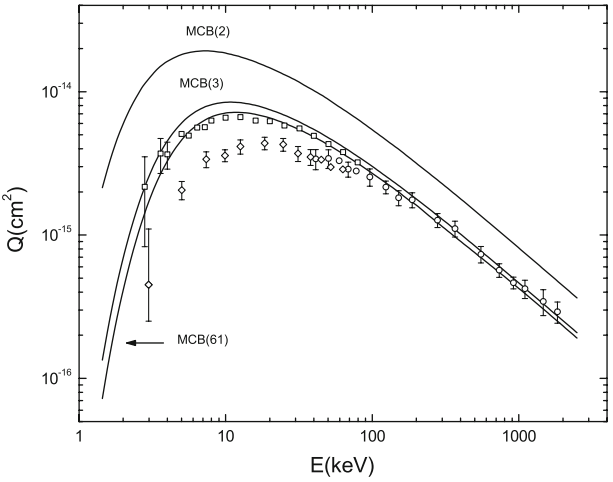

Fig. 5 Total cross sections Q as a function of the incident energy E for process (3.4). Theory: *full curves* (MCB method [49,50]). Integer N with the acronyms is the number of variational parameters in the target CI wave function from Silverman et al. [97] ($N = 2, 3$), as well as from Joachain and Terao [96] ($N = 61$). Experiment: *circle* [87], *diamond* [89] and *square* [101]

Under these circumstances, the prior transition amplitude $T_{if}^{(\mathrm{MCB})-}$ becomes computationally easier to handle than its post counterpart, $T_{if}^{(\mathrm{MCB})+}$. As such, in this Section, the remaining illustrations will be based upon computations that employ exclusively the prior total cross sections.

Convergence of the cross sections $Q_{if}^{(\mathrm{MCB})-}$ as a function of the electronic correlations is shown in Figs. 5 and 6. As can be observed in Fig. 5, the results for the 2-parameter $(1s1s')$ radially-correlated wave function of Silverman et al. [97] are significantly different from the other two curves that take into account the radial and angular correlations. It should be recalled that the angular correlation terms ($l_i' \neq 0$) of the wave functions with $N = 3 - 61$ parameters [95–97] are not explicitly present in $T_{if}^{(\mathrm{MCB})-}$ from (4.2). As discussed, they are implicitly included via the variational parameters as well as the binding energy E_i that differ for the wave functions comprised solely of the pure s-functions ($l_i' = 0$) and those for a mixture of orbitals with $l_i' = 0$ and $l_i' \neq 0$. It is obvious from Fig. 5 that there is a huge improvement in the cross sections $Q_{if}^{(\mathrm{MCB})-}$ when passing from the 2- to 3-parameter wave functions i.e. from the $(1s1s')$ orbital (radial correlations only) to the $\{(1s1s'), (2p)^2\}$ configuration (both radial and angular correlations) of Silverman et al. [97], respectively. This proves a strikingly important role of the angular correlations. A further illumination of this latter effect is evidenced by using the highly-correlated CI wave functions of Tweed [95] with 21–41 parameters, as well as of Joachain and Terao [96] with $N = 61$. The corresponding results displayed in Figs. 5 and 6 illustrate fast convergence of the cross sections $Q_{if}^{(\mathrm{MCB})-}$ as a function of the systematically increased degree of correlations. This is yet another appealing feature of the MCB method.

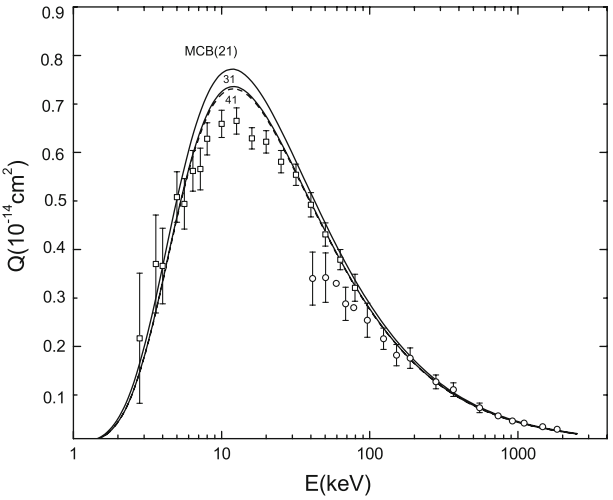

Fig. 6 Total cross sections Q as a function of the incident energy E for process (3.4). Theory: *full curves* (MCB method [49,50] with $N = 21, 31$) and *dashed curve* (MCB method [49,50] with $N = 41$). Integer N with the acronyms is the number of variational parameters in the target CI wave function from Tweed [95] ($N = 21, 31, 41$). Experiment: *circle* [87] and *square* [101]

Comparisons between theory and experiment in Fig. 5 show that the cross sections $Q_{if}^{(\mathrm{MCB})-}$ obtained with the 2-parameter radially correlated orbital [97] overestimate the experimental data by a sizeable factor ranging between 2.9 and 1.6 in the impact energy interval $E \in [26.03, 918.06]$ keV. Still, the overall shape of the theoretical curve is adequate at all energies, yielding qualitative agreement of theory with the measurements. However, a substantial improvement in $Q_{if}^{(\mathrm{MCB})-}$ giving highly satisfactory, quantitative agreement with the experimental data is obtained by employing the 3-parameter radially and angularly correlated orbital [97]. Remarkably, as seen in Fig. 5, the simple 3-parameter $\{(1s1s'), (2p)^2\}$ CI wave function [97] is able to bring the MCB method into a quite good agreement with the measurements. Overall, both the 2- and 3-parameter orbitals [97] lead to the cross sections $Q_{if}^{(\mathrm{MCB})-}$ that are either in qualitative (2-parameter) or quantitative (3-parameter) agreement with the Bethe asymptotic formula $\propto (1/E) \ln (E)$ at high impact energies E.

Despite this achieved success, further quantitative improvement of the MCB method is still needed in the extended region (5–100 keV) around the Massey peak [10], as seen in Fig. 5. The experience with the 3-parameter orbital [97] indicates that the sought improvement of the MCB method could be accomplished by utilizing the highly correlated many parameter (21–61) CI wave functions [95,96]. The resulting cross sections depicted in Figs. 5 and 6 achieve this goal. The completely converged results $Q_{if}^{(\mathrm{MCB})-}$ obtained with the 61-parameter orbital [96] are seen in Fig. 5 to be in perfect agreement with all the experimental data from the threshold, through the whole region of the Massey maximum [10] to large impact energies characterized by the dominance of the Bethe asymptote $\propto (1/E) \ln (E)$.

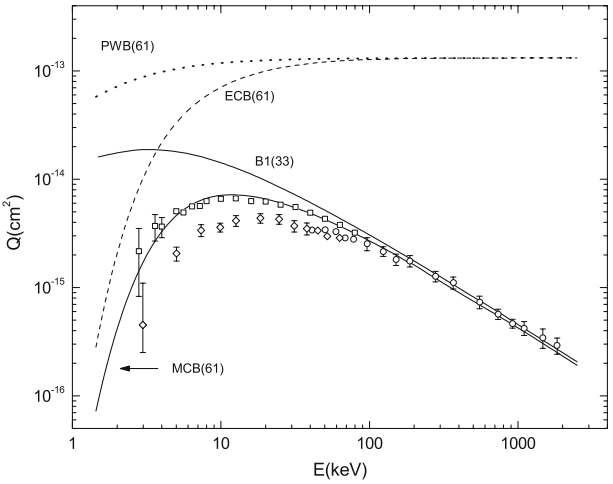

Fig. 7 Total cross sections Q as a function of the incident energy E for process (3.4). Theory: *dotted curve* (PMB method [79] with $N = 61$), *dashed curve* (ECB method [79] with $N = 61$), *upper full curve* (B1 method [80] with $N = 33$) and *lower full curve* (MCB method [49,50] with $N = 61$). Integer N with the acronyms is the number of variational parameters in the target wave function from Joachain and Terao [96] ($N = 61$) as well as from Rotenberg [102] ($N = 33$). Experiment: *circle* [87], *diamond* [89] and *square* [101]

Having carried out the detailed analysis and discussing separately the overall performance of the ECB and MCB methods, we can now perform direct comparisons between these two approximations. The results of such comparisons are given in Figs. 7 and 8 which also include the related total cross sections computed by means of the PWB, B1, AO and MO methods. The experimental data are plotted in Figs. 7 and 8 for the purpose of seeing the overall performance of the other theoretical models such as the PWB, B1, AO and MO methods.

As a direct consequence of including all the Coulombic effects of free charged particles in both channels of process (5.1), the total prior cross sections $Q_{if}^{(\mathrm{ECB})-}$ from the 61-parameter $(1s1s')$ radially correlated wave function $\varphi_i(\boldsymbol{x}_1, \boldsymbol{x}_2)$ [96] are seen from Fig. 7 to be considerably smaller than $Q_{if}^{(\mathrm{PWB})-}$ at low energies. In a previous study, Geltman [76] reached a similar conclusion using the PWBO approximation, which is empirically modified to include the simplest form of Coulombic effects through the Coulomb normalization factor in the entry channel. Further, it can be observed in Fig. 7 that at intermediate and high energies, the results $Q_{if}^{(\mathrm{ECB})-}$ and $Q_{if}^{(\mathrm{PWB})-}$ are very similar and they both possess the same constant value for their asymptotic limit, rather than the correct Bethe formula $\propto (1/E)\ln(E)$ for large E. Such an occurrence represents the most severe consequence of the inconsistency between scattering states and perturbation potentials within the ECB method.

The experimental data of Peart et al. [89] became available in 1976 for single electron detachment from H^- by proton impact as in process (3.4). This measurement revealed that the ECB model overestimates the experimental total cross sections Q by two orders of magnitude at energies E between 2.98 and 70.40 keV, as can be seen in

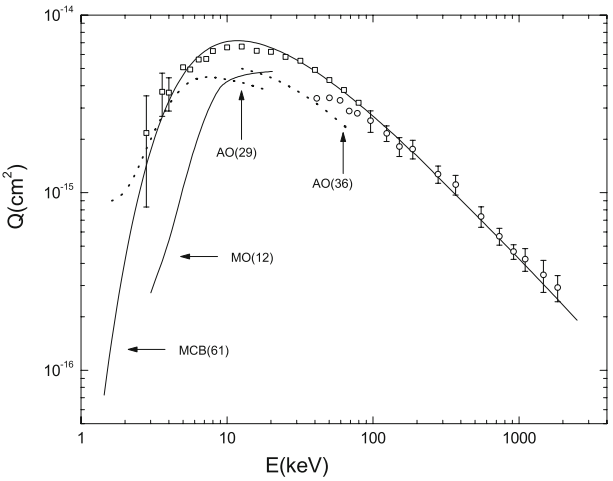

Fig. 8 Total cross sections Q as a function of the incident energy E for process (3.4). Theory: *dotted curves* (AO method [83] with $N = 29, 36$), *lower full curve* $E \in [3, 20]$ keV (MO method [81] with $N = 12$) and *upper full curve* $E \in [1.4, 2498]$ keV (MCB method [49,50] with $N = 61$). Integer N with the acronyms is the number of variational parameters in the target CI wave function from Joachain and Terao [96] ($N = 61$) as well as from atomic [83] ($N = 29, 36$) and molecular [81] ($N = 12$) orbitals. Experiment: *circle* [87] and *square* [101]

Fig. 2. As discussed, this discrepancy could have also been inferred by means of the earlier experimental data of Peart et al. [89] from 1970 on the $e + \mathrm{H}^- \longrightarrow e + \mathrm{H} + e$ collisions provided that the incident energies are scaled (see Figs. 1, 2, 5, 7). The experimental data from [89] extends to 918.06 keV of the equivalent proton energy, at which the ECB model exceeds the experimental findings by three orders of magnitude, as can be seen in Figs. 2, 5 and 7. The reason for such an unprecedented discrepancy was not known until 1997 when the problem was revisited by Belkić [49,50] who found that the distorted wave χ_i^+ and the distorting potential $V_{\mathrm{ECB}} = -1/s_1$ (with or without ΔV_{P_2}) in the entrance channel are not mutually consistent. The correction of this latter potential enabled the emergence of the MCB method [49,50] as the most adequate theory to date for the detachment process (3.4). The total cross sections $Q_{if}^{(\mathrm{MCB})-}$ computed with the same 61-parameter wave function φ_i from [96] are observed in Fig. 7 to be 2–3 orders of magnitude smaller than $Q_{if}^{(\mathrm{ECB})-}$. Furthermore, these two latter cross sections have a completely different dependence on the impact energy E. The difference between the ECB and MCB methods becomes most dramatic at larger values of E for which $Q_{if}^{(\mathrm{MCB})-}$ exhibits the proper asymptotic behavior $\propto (1/E)\ln(E)$, in contradistinction with the constant limiting value of $Q_{if}^{(\mathrm{ECB})-}$. Most importantly, the MCB is in perfect agreement with the measured cross sections at all energies, including the experimental data of Melchert et al. [101] from 1999. At the same time, the ECB model totally fails despite the use of the most correlated 61-parameter wave function. Such a conclusion from Figs. 2 and 7 disproves the claim by Bell et al. [80] that the ECB is unsuccessful in comparison with the measurements because Gayet et al. [79] employed the simple 2-parameter wave

function [97]. In Fig. 7 we also display the cross sections $Q_{if}^{(\mathrm{B1})-}$ in the B1 method computed by Bell et al. [80]. As anticipated, the cross sections of the MCB and B1 methods are in a close mutual agreement at sufficiently high energies (above 150 keV), since they both contain the correct Bethe limit. The curve presenting the B1 method of Bell et al. [80] was obtained by employing the highly correlated 33-parameter wave function φ_i of Rotenberg and Stein [102]. The cross sections $Q_{if}^{(\mathrm{B1})-}$ from Fig. 7 significantly overestimate the experimental data at energies below 30 keV, where the attractive Coulomb potential between the projectile H^+ and target H^- is strongest. This occurs because a slow incident proton spends more time in the vicinity of the target. Thus, to overcome the inadequacy of the B1 method, especially at lower and intermediate energies, it is necessary to include at least the Coulomb effects between H^+ and H^- in the entrance channel. The MCB method achieves this in a remarkably complete manner as seen by comparing the B1 and MCB method in Fig. 7. Overall, the MCB method appears as highly adequate due to the full reproduction of the two mutually coherent sets of experimental data from [89] and [101]. This comes as a direct consequence of the internal consistency of the MCB method via (i) the initial and final scattering states with the correct asymptotic behaviors, as well as (ii) the adequate distorting perturbation potentials in the entrance and exit channels with their proper links to the associated wave functions. When only part (i) of the correct boundary conditions in the entrance channel is fulfilled, the ECB method is obtained, but the outcome of the missing part (ii) is a dramatic disagreement of this latter theoretical model with all the available experimental data. However, the simultaneous fulfilment of the requirements (i) and (ii) gives the MCB method with the ensuing remarkable success at all impact energies. The least satisfactory situation is in the B1 method where neither the initial scattering wave function Φ_i nor the perturbation interaction $V_i^{(\mathrm{B1})}$ in the entrance channel is correct. This happens because at $R \to \infty$, the interaction $V_i^{(\mathrm{B1})} \equiv 1/R - 1/s_1 - 1/s_2 = \Delta V_{\mathrm{P}_2} - 1/s_1 \approx -1/s_1$, which produces the transition in the prior T-matrix element $T_{if}^{(\mathrm{B1})-}$ in the B1 method, represents an attractive long-range Coulomb potential $(-1/s_1)$ between the incident proton and the active electron e_1 to be emitted. This is not consistent with the fact that the entrance channel wave function in the B1 method is described by the unperturbed state Φ_i, which is adequate only if $V_i^{(\mathrm{B1})}$ were a short-range potential.

In Fig. 8, the MCB method is compared with the AO or MO methods. The AO and MO methods, as the close coupling approximations, use reasonably large atomic or molecular basis sets of the expansion functions. Ermolaev [83] used 29 and 36 atomic orbitals, whereas Sidis et al. [81] employed 12 molecular orbitals to solve the close-coupling system of ordinary differential equations. It is seen in Fig. 8 that the AO method [83] with 29 orbitals partially reproduces the measured cross sections at very low energies near the threshold. However, at intermediate and large values of E, the experimental data are underestimated by the AO method with 36 orbitals [83]. Moreover, the cross sections from the AO method with 29 and 36 orbitals do not converge to each other in the overlapping energy region around the Massey maximum. Further, the AO and MCB methods are in good mutual agreement only in a very limited energy range 1.5–4 keV. On the other hand, the MO method largely underestimates the experimental data at all energies 3–20 keV covered by the computations from [81].

As can be seen in Fig. 8, the curves of the MO and MCB methods are nearly parallel at most of the overlapping energies, but the cross sections of the former method are lower than those due to the latter method. As such, the MO method underestimates the measured data by a factor ranging from approximately 7 at 3 keV to about 2 at 10 keV.

Overall, our analysis of process (3.4) in this Section firmly demonstrates the need for great care in establishing a proper link between the long-range Coulomb distortion effects and the corresponding perturbation potential. If this is overlooked, utterly unphysical results could easily be obtained, as actually was the case in the work of Gayet et al. [79]. Additionally, as evidenced by Fig. 5, the discussed results clearly demonstrate that perfect quantitative agreement between the MCB theory and the available experimental data at all impact energies can be obtained by employing the bound-state wave functions of the $H^-(1s^2)$ target with a high degree of static inter-electron correlations.

6 Prospects for medical applications of continuum distorted waves

Thus far, we analyzed the most salient aspects of ionization in ion-atom collisions within the continuum distorted wave formalism. The main features of this general methodology are of relevance to several important applications of ionizing collisions, including fusion research [103], hadron therapy [104–119], etc. We shall focus our discussion on the major aspects of high-energy ion-atom collision theory of potential relevance to modeling of the passage of ions through tissue and tissue-like media as needed in hadron therapy. Our overall goal is to highlight the possibilities that will improve the atomic physics cross section data bases as entries to MC simulations of energy losses during ion transport in tissue. Before elaborating the way in which this could effectively be achieved, it is important to state the reasons for which this task should be formulated in the first place. To this end, it is deemed necessary to contextualize the planned strategy by giving a selected pertinent extract of hadron therapy.

6.1 Role of atomic collision physics in modeling of ion transport through tissue

Radiotherapy or radiation therapy, is a general therapy for various ionizing beams used in clinics not only for tumor eradication in patients with cancer, but also for some non-malignant disorders. Radiotherapy can be delivered by external beams or administered internally (brachytherapy) by injection of radioactive sources. We shall discuss only the external radiotherapy, calling it hereafter radiotherapy. It is customary in medicine that radiotherapeutic ions with nuclear charge $2 \leq Z_P \leq 10$ are called light ions, although this is an arbitrary terminology. In order to conform with this medical terminology, the term 'light ions' will hereafter exclude nuclei with charge $Z_P > 10$. Therefore, it should be useful to highlight some of the main radiotherapeutic features of ion beams [108]. Both biological and physical aspects of ion beams are essential for radiotherapy, but our extracts from this subject will be concerned primarily with physical properties.

Cancer is not a single disease, but rather it is a group of diseases. Moreover, there are about 100 different types of cancers. Their common denominator is an uncontrolled growth of malignant or clonogenic tumor cells. The latter cells are those that have undergone mutations i.e. genomic changes. In principle, most cancers can be curable, with varying degree of success, depending on many factors, including the type of tumor, early detection, location, the presence of metastasis, etc. Cancers and cardiovascular diseases are the two leading causes of human deaths worldwide. Cancer incidence is increased in most recent times for many reasons.[5] A recent study [120] on the proportion of cancer incidence and cancer deaths in Europe revealed that only in 2004 some 2.9 million new patients with cancer were diagnosed, and about 1.7 million deaths from cancer occurred. The most recent report from 2008 by the cancer expert group in the International Atomic Energy Agency (IAEA) [121] estimates that the chance of dying from cancer is within the range 20–25% for people living in the industrialized European countries. Overall, the epidemiological data, statistical estimates as well as predictions indicate that cancer is a major problem area for public health. On the other hand, due to cancer complexity, this area is highly multi-disciplinary to which physics can contribute substantially.

Physicians consider that the key to fighting solid malignant tumors is control through removal by surgery or inactivation by various treatments such as chemotherapy, radiotherapy, immunotherapy, gene therapy, hormone therapy, etc [121]. Thus far, the most common clinical strategies in fighting cancer are surgery, chemotherapy and radiotherapy. Some 60% of patients with cancer undergo radiation therapy and it is often stated that about half of them are cured. However, such statements are currently lacking data on risks for long-term complications such as recurrences and secondary cancers. Radiotherapy is usually administered through fractionated treatment of patients within one month every second day to allow repair of damaged healthy cells. It is frequently stated that most tumor cells are irreparably damaged by irradiation. This is accompanied by estimates that most normal healthy cells can repair irradiation damage within 24 h, and this presumably justifies fractionated therapy. Of course, both statements are of a statistical nature stemming from in vitro studies on irradiation of tissue cell lines. Any use of such in vitro findings in attempts to draw definite and firm inferences on patients should always be taken with precautions. In this context, it is important to have a simple quantitative and comparative sense about the ionizing power for different radiation modalities. To this end, let us imagine some 1000 living cells exposed to 1 rad or 0.01 Gy photons, which is equivalent to the amount of radiation used in one spinal examination by X-rays. This target would suffer about 100000 ionizations of the incumbent deoxy-ribonucleic acid (DNA) molecules within the whole colony of cells or roughly from 11 to 460 ionizations per cell. The biological effect of this radiation exposure would be 2–3 cell deaths, but also 2–3 cell mutations or irreparable cell damages in DNA. Relative to this, e.g. alpha particles delivering a comparable dose would produce 3700–4500 ionizations per cell leading to 10 times more cell deaths and, of course, as many cell mutations or irreparable damage in DNA. Expectedly, carbon nuclei would produce many more dense ionizations leading to considerably

[5] More and more people are diagnosed with cancer also because modern detection modalities are more effective than the ones from the past.

more tumor cell killings and mutations or irreparable damages of tissue DNA molecules. If instead of this example with colonies of living cell lines from a biopsy, one considers a patient, the clinical oncologist would strive to strike a delicate balance in weighing potential benefits (tumor cell deaths) against risks (mutations and/or irreparable normal cell damage). For quantitative and reliable risk assessments, thorough interdisciplinary preclinical and clinical research activities are necessary encompassing physics and biochemical studies on repercussions of short- and long-term effects of irradiation of patients. In general, clinical oncologists are conservative regarding any new radiation modality. For them, it is not enough to see a demonstrable superior dose delivery to the intended tumor target, while simultaneously sparing the healthy uninvolved tissue, as is actually the case e.g. for light ions relative to photons. This stance is due to intertwining of tumorous and healthy tissues at the target, but also to the unavoidable damage to normal tissue from the entrance all the way to the target. Such circumstances lead to the key inquiry beyond the argument of a favorable dose distribution as a function of depth: how many of the irradiated normal cells would be able to repair, and even when they do, could such repairs prevent secondary, radiation-induced cancers?

Despite the available biophysical evidence about advantages of dose-depth distributions of protons relative to the conventional modalities in therapy and regardless of a steadily growing number of proton accelerators for radiotherapy, it is intriguing to see that considerable controversy is still present as to whether even protons (let alone heavier nuclei) should be widely adopted in clinical use [122–131]. This is because serious concerns are being raised in the literature with the pros and cons about the need for randomized clinical trials in evidence-based medicine. Randomized clinical trials are needed and ethically justified if the knowledge about certain major issues is lacking and estimates on benefits versus risks are uncertain.[6] As stated earlier, the relatively unknown long-term side effects of radiotherapy, such as radiation-induced cancers represent major issues of clinical concern. Both of these concerns could partially be addressed through longitudinal studies by including a large number of confounding factors and performing a comparative multivariate analysis e.g. for proton and photon therapies. This would be entirely feasible provided that follow-up data exist for cancer patients treated by protons and photons. However, according to [131], no data are available on late morbidity (e.g. more than 10 years after the treatments, and this is especially relevant for children) for patients who underwent photon or proton therapy. One of the expected answers from such longitudinal studies would be an assessment of the level of the relative risks for secondary cancers after irradiation by protons and photons. As stated, an initial indication on this is provided by comparisons of dose planning systems showing that the healthy tissue is irradiated more by photons than protons. Therefore, the risk for secondary cancers is expected to be higher for the former than for the latter therapy, but the statistical significance of these differences is largely unknown and needs to be determined. In a randomized clinical trial aimed at assessing the relative effectiveness for the possibility of cancer curing by a conven-

[6] Additionally, all health care systems have other important issues to consider for each new/alternative treatment modality, such as the relative cost-effectiveness, patient referrals, reimbursement by medical insurance, etc.

tional and non-conventional therapy for those for whom both modalities are indicated, the oncologist must inform the patients that one modality will irradiate the healthy tissue more than the other, while simultaneously depositing less or at best equal dose to the tumor itself.[7] Moreover, the patients must also be informed that it will be decided at random whom will be treated by the conventional and whom by the non-conventional therapy. These and other important issues of the protocols are necessary in the process of trying to get the consents from the patients who are ultimately the ones to decide whether or not to submit themselves to a therapeutic modality with a possible higher risk than the other alternative which they would miss at random. How many patients could oncologists hope to have for a randomized clinical trial focused on photons and protons, after the patients were informed about their higher risks for secondary cancers in the case of photon therapy? Current debates with arguments and counter-arguments for randomized clinical trials for proton therapy are ongoing [130,131], and this will probably be the case in the near future even more so for heavier nuclei such as those from lithium, carbon or oxygen atoms, should these ions have a chance for worldwide spreading. Suit and Kooy [131] emphasize that several conventional therapies such as single and multiple fields, wedge and compensator filters, linear accelerators and intensity modulated radiotherapy (IMRT) have not undergone the scrutiny of evidence-based medicine via randomized clinical trials. These authors [128,131] state that the mentioned therapies were clinically approved solely on the basis on their demonstrable superiority and benefit from the improved dose planning systems. However, according to Schulz and Kagan [130], such a practice of bypassing randomized clinical trials by exclusive reliance upon favorable dose distributions (even if they are nearly ideal) should not be continued with hadron therapy. To support their stance, these authors cite the presumably still missing clinical proof-of-principle for hadron therapy, cost-effectiveness, significant increase in treatment capacity, etc. Naturally, citing only the need to assess cost-effectiveness of hadron therapy would not motivate patients to whom an extended list of rationales needs to be presented to obtain their consents for participation to randomized clinical trials [131]. Evidence-based medicine, where randomized clinical trials rank high, is among the priorities of health care authorities that are conservative when it comes to clinical approval of hadron therapy for wide adoption based solely on the improved dose distributions and better biological effects. But how much better and to what extent do these biophysical ameliorations indeed translate into the distinct clinical benefit for patients versus eventual post-therapeutic complications (recurrences, secondary cancers, radiation-caused cardiac morbidity, etc) remains to be determined, and these are among the major concerns of physicians and health care authorities. Such trials could have been carried out in the 1990s at the first dedicated proton therapy center in Loma Linda in California. This was not done. More recently, the argument for performing the needed clinical trials was one of the main driving forces that clinched the approval for construction of the first Swedish hospital-based facility for proton therapy in Uppsala (planned to run in 2012) [122]. Additionally, more than 20 similar, dedicated radiotherapeutic facilities are planned

[7] Here, non-conventional does not necessarily imply new. An example of the conventional and non-conventional therapy is photon and proton therapy, respectively. Of course, proton therapy is hardly new, since it is in clinical use worldwide for a long period of time.

to be built in the next decade in several countries. This should significantly improve the chance for clinical trials for which the realistic possibilities were minimal or non-existent earlier with insufficient beam-times at university-based accelerators assigned primarily to physics projects.

Surgery and radiotherapy are in some cases advantageously combined. Also non-surgical modalities are combined e.g. radiotherapy is often used after chemotherapy. Ideally, removal or inactivation should be as complete as possible to avoid recurrences. To tend closely to this ultimate goal of attempting to cure patients by surgery and/or radiotherapy, the following four conditions are critical inter alia:

- early detection of tumor,
- precise target delineation,
- optimal beam control and
- post-therapeutic follow-up.

Early detection via screening as well regular and systematic medical examinations greatly increases chances for a fuller control. Vital to both the early detection and target definition are a variety of medical imaging diagnostics that are also used for evaluation of patient follow-up in post-operative or post-therapeutic stages, such as magnetic resonance imaging (MRI), magnetic resonance spectroscopy (MRS), magnetic resonance spectroscopic imaging (MRSI), computerized tomography (CT), positron-emission tomography (PET), single photon emission computerized tomography (SPECT), ultrasound, etc [132].

From the clinician's viewpoint, the overriding feature is control when comparing different radiation modalities (photons, electrons, protons or other ions). Oncologic surgeons strive to achieve control by trying to minimize removal of neighboring healthy tissue, which is often intertwined with the complicated topology of tumorous tissue. Radiation oncologists attain control by adequate dose[8] planning systems and treatment plan. This should secure (with a reasonable certainty) the implementation of the concept of target conformity. This concept is defined by the goal that the dose is delivered directly to the tumor mass and to the adjacent volume which is at risk for micro-extensions of tumor, while simultaneously sparing the healthy tissue. Such a goal is approximately achieved by putting certain technical constraints to the applied radiation modality, so that it eventually conforms to the overall topology of the tumor. In other words, the aim is to achieve a sufficiently high degree of spatial agreement i.e. conformity between tumor boundaries, within a certain margin, and the corresponding irradiation coverage. These constraints lead to various devices known as multi-leaf collimators (MLC), stereotactic treatments, IMRT [133], etc.

On- and off-beamline PET-CT cameras, that combine PET and CT, can be used to monitor the location and distribution of the delivered dose at the tumor site[9] [134–137]. Thus far, on-line PET-CT has been used for those ionic projectiles that after fragmentation (via nuclear reactions with tissue) can create positron emitting isotopes. An example is the $^{12}C^{6+}$ primary beam (currently used as radiotherapeutic ions

[8] Dose is the energy deposited per unit mass, expressed in grays (Gy = J/kg).

[9] On-beamline means that the PET-CT camera is built in the beamline so that treatment verification can be made during irradiation of the patient. Off-beamline dose delivery control with PET-CT camera is done after the irradiation.

in Germany and Japan), which can undergo transmutations in collisions with tissue, leading to unstable isotopes $^{11}C^{6+}$ and $^{10}C^{6+}$ that are positron emitters [134–136]. Off-line PET-CT for primary beams of protons is currently under testing in the US on typical tissue-equivalent phantoms [137] prior to the envisaged clinical use. By design, PET-CT cameras rely on positron-electron annihilation to operate. However, no primary beam fragmentation occurs when protons are used as radiotherapeutic ions. Nevertheless, protons can lead to target fragmentation which, it turn, could yield some positron emitting nuclei that would enable PET-CT to function [137].

Ever since the publication of Wilson's ground-breaking paper in 1946 [138] (see also [139] for details of modeling and computations), where he explicitly envisaged the use of protons, alpha particles and carbon ions in radiation therapy of patients with cancer, deep interest of oncologic surgeons and radiation oncologists for these non-conventional treatments grew steadily and worldwide. The first humans were treated (hypophysectomy and pituitary gland) by 340 MeV proton and 190 deuteron beams as early as 1954 in Lawrence Berkeley Laboratory, US [140–143]. The deuteron beams from this latter study were also used for irradiation of the hypophysis of animals in 1958 in Uppsala, Sweden [144,145]. Nevertheless, protons made a long journey from physics accelerators to hospitals in the course of passing the test of time. It was not until the 1990s in the US that proton beam therapy finally became feasible clinically in the hospital setting, thus presenting itself as a potential integral part of the armamentarium of radiotherapeutic modalities. Thus far about 40000 patients had been treated by proton therapy and numerous satisfactory outcomes were recorded for certain tumors [108]. Alpha particles and neon ions have also been tried for radiotherapy in the US in the 1980s, but these investigations have not been completed due to discontinuation of funding. However, the subsequent decade witnessed carbon ions undergoing vigorous testing, which was deemed successful and these new beams have been accepted clinically in Germany and Japan where altogether some 4000 patients have been treated since 1997. Moreover, several other European countries (Italy, France, Austria, Sweden) have either investigated the possibilities or begun constructions of hospital-based accelerators to complement protons with high-energy light ions for radiotherapy of deep seated tumors.

One wonders, what was the reason for a delayed entry of proton beams into treatments rooms of hospitals and why is the use of other heavier ions still relatively scarce?

Physicists may come up with well-rounded proposals for various ions in radiotherapy, but as Wilson rightly admitted, the ones who ultimately take the decision must be physicians. However, as mentioned, physicians are understandably conservative when it comes to new radiotherapeutic modalities because of an overriding concern, which is care for patients' well being and safety dictated by the golden rule of medicine '*primam non nocere*' (above all do no harm). Clinicians ultimately approved electrons and photons for cancer treatments, but any other proposed modality is evaluated in the light of potential new risks for patients relative to the conventional radiotherapy [123–131].

There are three major reasons for which protons waited for nearly five decades since Wilson's original proposal before making their use in clinics at hospital sites:

(i) with the insufficient technological possibility to secure a highly accurate target delineation in the 1980s, protons' theoretical advantages relative to electrons and photons could not be fully exploited in the clinical practice,
(ii) proton accelerators being dedicated to physics projects were too costly to be run for clinical purposes alone,
(iii) technology for medically dedicated proton accelerators in the hospital settings was not available until the 1990s.

For light ions, the necessary technology presently exists, but the initial investments into the related ring accelerators dedicated wholly to medicine are considerably higher, so that potential investors and national programs exercise noticeable caution and hesitation. More importantly, each new ion beam must undergo rigorous investigations for assessing, as thoroughly as possible, the potential biological responses of various tissues to exposure to these radiations. Here, no computational simulation, however detailed it might be, could by itself be considered as sufficient, unless complemented by at least 3–4 years of thorough biological measurements for each newly proposed ion beam for radiotherapy. Besides protons, such stringent criteria have thus far been met only for carbon ions $^{12}C^{6+}$ among all the other ions that were and still are the possible candidates for radiotherapeutic beams.

Vigorous debates are currently under way in several European countries and many researchers seem to be strongly polarized around protons and light ions. Those who are for protons criticize high initial costs of medical accelerators for light ions, pointing at the arguably successful test of time passed by protons. Those who are for light ions, claim that the initial investment costs are admittedly high for building medically dedicated accelerators from the onset for these beams, but argue that what would subsequently follow could be more cost effective for new facilities. They add that light ions cannot possibly pass the test of time if they keep being denied the chance to be scrutinized in the first place on a larger scale of the charge/mass ratios than what is currently in use (protons and carbon ions only). These debates could significantly be advanced if supplemented by suggestions on the feasibility studies with the purpose of making the initial assessments of potential therapeutic performance of other light ions with nuclear charges $Z_P \neq 1$ and $Z_P \neq 6$ at the already existing high-energy accelerators dedicated to physics per se. As mentioned the first patients were treated by protons in 1954 at physics facilities with adapted treatment rooms, and only years later in the 1990s, were medically dedicated proton accelerators constructed at hospital sites. Such a long waiting period for protons was due to lack of the appropriate technology, as stated. However, the needed technology is nowadays available for practically every possible ion beam, so that the waiting period for ions would depend only upon their having successfully passed the initial test in radiobiology during e.g. 3–4 years at physics facilities as reminiscent of the similar scientific and clinical scrutinizing of protons and carbon nuclei. This step-wise approach, if successful for radiobiological testings, is more likely to eventually justify subsequent constructions of medically dedicated accelerators for light ions at hospital sites worldwide rather than being currently limited to only a few countries.

Photon, electron and ion beams have in common the feature of being ionizing radiation modalities. They are used in the first place because of their ability to destroy,

primarily through ionization, the DNA molecules as the main producer of clonogenic i.e. tumorous cells. However, in doing so they also damage to a varying degree everything else on their way to the tumor site (which is their final destination), including the healthy tissue from the entrance into the body to the target and beyond. Despite all the precautions, including sophisticated optimization via conformal treatment aimed at disabling the diseased and preserving the healthy tissue at the target, damage to normal cells is unavoidable. This can manifest itself in a number of immediately apparent and undesirable side effects in patients e.g. vomiting, diarrhea, nausea, bleeding, painful sequelae, etc. Moreover, some consequences to the exposed ionizing radiation are of longer terms and could take years until they make their appearances. For example, investigations of radiation effects on cytokinic phenomena, such as cytokine activation, suggest that low dose radiation may lead to certain late sequelae e.g. excessive scar-tissue formation, increased risk of second tumor and the like.

Irrespective of belonging to the category of early or late sequelae, all the radiation side effects occur because normal cells receive more dose than they could tolerate. Moreover, each patient reacts in an entirely individual way to radiation, such that a general treatment plan may work for one and fail for the other patient with the same type of tumor. That is why radiation oncologists must always try to have a treatment plan for each patient so as to minimize the mentioned radiation side effects. Biological input to each patient's data base is critical for treatment plans that should anticipate as much as possible the major responses of the individual patient to radiation. Ultimately this would enable establishment of biologically optimized radiotherapy with ions [146].

All individual particles from the therapeutic beams carry energy which can be deposited anywhere on the way to the target. Too much deposited energy to healthy cells may result in their death. Even worse, an overdose can lead to cell mutations inducing new cancer in previously healthy tissue. Damage to normal tissue cannot be avoided, but could be hoped to be kept under a reasonably tolerable level. This tolerance level is conventionally conceived as the lowest total dose received by healthy cells such that repair of the damage is possible, resulting in re-establishment of normal functioning of these cells.

In 1946, Wilson [138] had a great vision stated as follows: "It will be possible to treat [by beams of protons and other ions] a volume as small as 1.0 cm^3 anywhere in the body and give that volume several times the dose of any of the neighboring tissue." He therefore foresaw in ions the opportunity offered to clinicians for an increased disease control with considerably diminished damage to healthy tissue. Highlighting succinctly the main physical features of ion beam transport through tissue, Wilson argued that these particles should help clinicians to arrive at their ultimate goals of achieving a superior control of the delivered dose relative to the conventional radiotherapy by photons and electrons. Subsequent intense studies on both animals and humans already in the period 1954–1958 have proven Wilson correct. For example, Larsson et al. [144] reported: "With a narrow proton beam it is therefore possible to produce sharply delineated lesions of a desired site in any region of choice in the central nervous system." And they concluded by giving the clinically most important caution: "It must be stressed, however, that the [above] observations apply only to lesions in their relatively early stages". Hence the critical role of early detection [147–152].

6.2 Major ion-tissue interactions in high-energy collisions

When ions enter the tissue, they are said to be transported through it up to a certain distance (called range R) which is determined primarily by the initial energy E of the projectile beam, its energy loss, range straggling and multiple scattering [153,154]. Ions lose their energy because they collide with the constituents of the traversed tissue. Due to their heavy mass, which is about $2000N$ times larger than the electron mass ($N \geq 1$ being the number of protons and neutrons in a nucleus), ion trajectories deviate only slightly from their incident directions. In other words, they scatter mainly in a narrow forward cone ($\theta_i \approx 0$). Many small angle scatterings occur while the ions pass by atoms/molecules of the encountered tissue. Such a cumulative effect is called multiple scattering and this phenomenon is more enhanced in thicker than in thinner targets. A beam contains a large number of ions and this leads to certain statistical effects. One of them is range straggling, which represents fluctuations in the range of individual ions. All the ions of the same energy do not attain the same range, since their collisions (by which they produce many secondary particles along their paths) are of a probabilistic/statistical rather than deterministic/preassigned nature. Thus, such ions are viewed as straggling to reach their range. Hence the term "range straggling".

In particle transport physics, one of the most important observables that characterizes the penetration capability of particles is the stopping power, $S(z)$, which represents the loss of ion energy per unit of traversed pathlength along the particle track (z), as denoted by $S(z) \equiv -\mathrm{d}E/\mathrm{d}z$. At high incident energies $E \geq 350$ MeV/amu of interest for radiotherapy on deep seated tumors of the corresponding range of about ~ 25 cm, the main scattering events that lead to energy loss of ions are nuclear collisions and target ionizations. As mentioned, ions scatter mainly forward, meaning that their paths are practically straight lines along which they transfer their energy to the tissue which becomes ionized or excited (at high energies, probability for ionization is about three times larger than that of excitation). Ions deposit several times more energy at their range (i.e. in the vicinity of the Bragg peak) than elsewhere, and this inverse dose-depth distribution is in sharp contrast to electrons and photons [155–157]. The measurement of Bragg and Klimann [157] was the first to report that α-particles deposit nearly all their energy when they are about to stop i.e. very close to their range. Dose-depth distributions or profiles are the curves that display the stopping power $S(z)$ as a function of depth z. A dose-depth profile of an ion beam is mostly a plateau-like curve, which ends abruptly with a prominent maximum called the Bragg peak situated at the target position. By contrast, electrons and photons deposit maximum energy near the beginning of their track, so that afterwards their dose curves decrease with distance all the way up to the target which is tumor in radiotherapy [108]. The tumorous tissue needs to be destroyed to stop the uncontrollable production of clonogenic cells and ions can partially achieve this through nuclear and ionizing collisions with the tissue. However only some 30% of ionization of the tissue's DNA molecule is accomplished by direct hits of ions counting all the primaries, secondaries and ions of higher-order generations. The remaining 70% of ionization rate of DNA is achieved by the secondary δ-electrons that are produced by the impact of ions on tissue. If the electrons emitted from a target are sufficiently energetic to be able on their own to lead to further ionzations they are called δ-electrons.

6.3 Clinical significance of dose-depth profiles

As stated, for photons and electrons, function $S(z)$ is a declining curve with increasing z for most of the paths of these beams [108]. This means that photon and electron beams deposit most of their energy earlier on the passage through matter. In such a case, the targeted tumor would receive the least energy, whereas simultaneously the healthy tissue throughout the radiation pathway would be exposed to considerable radiation. Such an obstacle for photon and electron beams can be significantly mitigated by IMRT.[10] Nevertheless, photon IMRT beams still deliver more dose to uninvolved, healthy tissue in comparison with heavy ions. Moreover, heavy ions deliver more dose to the tumor than photons for the same beam energy. Even when the deposited energy is the same for these two beams, the healthy tissue throughout the beam pathway receives less radiation with protons than with photons.[11] This is expected to translate into a potential benefit for the patient as follows from a direct comparison of the two dose planning systems.[12] How much better for patients is proton relative to photon IMRT therapy is the subject of intense research [161–164]. The clinical significance of these relationships is that the tumor control probability is higher for protons than for photons and, at the same time, the former relative to the latter leads to lower normal tissue complication probability. Nevertheless, it is critical to assess benefits against the main potential post-therapeutic risks such as recurrences and radiation-caused cancers.

6.4 From shielding in space programs to hadron therapy

Manned space missions are concerned with radiation shielding and protection against galactic nuclei of varying charge from proton to iron. These nuclei are energetic and they easily penetrate space vehicles and, of course, the bodies of crew members. Here, there is a twofold problem (with the ensuing hindrance toward the space program for exploration of the Solar system): a high uncertainty about late effects of irradiation by fast heavy nuclei and the current lack of effective preventions against potential risks. Among the main risks are carcinogenesis, late degenerative tissue effects, hereditary consequences, etc. Risks can be reduced by studying the atomic and nuclear interactions of ionic radiation with matter in order to achieve a better shielding of rockets and humans.

There are no studies that could rule out with certainty severe long term side effects from medical therapy by ions and this is particularly relevant for deep-seated tumors. Deep penetration in tissue necessitates very energetic ions of a few hundreds of MeV per nucleon. Such fast heavy particles readily undergo nuclear transmutations in tissue with abundant production of secondary particles, including neutrons, either from the beam fragmentation for composite incident nuclei or from the tissue targets. Several

[10] Photon IMRT is called X-ray IMRT by physicians.

[11] Recently, IMRT was designed for proton beams and this is called intensity modulated proton therapy (IMPT) [158–160], which is superior to photon IMRT especially regarding the increase in the dose gradient.

[12] Besides a dose planning system, there is also a treatment plan, which displays the distribution of the physical dose (in the units of Gy) versus the radiobiologic equivalent of 10% at the points of interest in the patient.

neutrons per one primary particles can readily be produced against which there could be no shielding in the patient's body, of course. Thus, Chaudhri [165,166] reported that each alpha particle or carbon nucleus colliding with tissue-equivalent materials produce, respectively, 2 or 4 neutrons at energies 200 or 400 MeV/amu that are used in radiotherapy of deep-seated tumors at depths close to 25 cm. This is correct for collisions of the type $^{4}He^{2+} - H_2O$ and $^{12}C^{6+} - H_2O$, as can easily be checked using the Bragg sum rule for water molecule (cross section Q_{H_2O} for H_2O deduced from the associated atomic cross sections Q_H and Q_O via $Q_{H_2O} = Q_H + 2Q_O$) and the corresponding known nucleon-nucleus total cross sections (elastic plus inelastic) for the reactions $^{4}He^{2+} - {}^{1}H^{+}$ and $^{4}He^{2+} - {}^{16}O^{8+}$ as well as $^{12}C^{6+} - {}^{1}H^{+}$ and $^{12}C^{6+} - {}^{16}O^{8+}$. At the mentioned high impact energies, nuclear collisions with the emergence of neutrons are the main channels of energy losses of ionic beams. These emitted neutrons can cause late effects, including new tumors years after treatment. Fragmentation tails beyond the prescribed range invariably appear for ions heavier than protons. This irradiation spillover can reach considerably farther distances beyond the targeted tumor, thus causing damage to healthy tissue with possibly induced cancers. Lighter secondary nuclei produced by transmutations of heavy ion beams have longer ranges and can disperse to larger scattering angles than the associated primary particles. Primary heavy nuclei scatter mainly in the forward direction, thus having practically straight tracks and limited lateral spreading or diffusion. Heavy ions possess inverse dose-depth profile relative to electrons and photons. As noted, the ultimate goal is to assure a conformal dose distribution which covers the tumor while, simultaneously sparing the surrounding healthy tissue. This presumes a very precise target definition in which diagnostics plays the pivotal role. Diagnostic modalities are used also in post-radiation follow-up. Here, as mentioned, especially MRS and MRSI are critically important for in-depth quantifiable wide-range metabolic information extracted non-invasively from the scanned tissue [147–152].

Clearly, space research and hadron therapy have vastly different scopes and priorities so that drawing parallels between these two disciplines is not possible or necessary. Nevertheless, space research and hadron therapy have shielding and radiation protection in common. Therefore, it is natural to seek a cross-disciplinary link for a better understanding of the physics basis of the biological action of heavy ions. Moreover, these two branches share similar methodologies of particle transport physics regarding both deterministic and stochastic theoretical descriptions. One of the good examples of this kind of cross-links between two branches is an adequate adaptation of the Monte Carlo (MC) simulation code SHIELD from its original inception in the shielding problems in space research to the corresponding variant SHIELD-HIT [117,118] for the purpose of heavy ion therapy (HIT). The nuclear physics part of SHIELD-HIT is preserved from the most recent version of SHIELD and, hence, this section of the algorithm is fully up to date. However, this is not the case for the associated atomic physics part, which can significantly be improved by using the CDW methodologies as the most adequate quantum-mechanical descriptions of inelastic ion-atom collisions at high impact energies. The motivation for this strategy is to have a fully adequate version of SHIELD-HIT from both nuclear and atomic physics standpoints. In order to make this strategy comprehensive, one has to simulate also transport of

δ-electrons alongside ions in tissue. Currently, SHIELD-HIT simulates only ion transport.

6.5 Key mechanisms in ionizing collisions

Of course, δ-electrons can also be produced by electron beams for which accelerators are much more affordable to a wider circle of potential users than those for ions. And since at any rate the δ-electrons are the dominant ionizers of DNA, one naturally wonders why electron beams are not directly used for production of the therapeutic δ-rays in the first place? The answer is in the fact that ion beams are much more effective in producing δ-electrons than primary beams comprised of electrons. The secondary electrons move in a combined Coulomb field of two centers located at the projectile and target nuclei. This two-center aspect of ionization leads to the Z_P^3- dependent mechanism through the ECC effects as an additional source of δ-electrons that are missing in the B1 [11–15] and Bethe–Bloch [16,17] formulae. The methods presented in the most recent reviews [3,4] can be used to explore the advantages of the atomic physics leading theories, notably the CDW [8,9], CDW–EIS [45–48] and MCB [49,50] methods that are capable of treating both nuclei on the same footing in ionization phenomena. Initial applications of these CDW methodologies to fast collisions involving water molecule as a target and heavy nuclei as projectiles have already been made with promising results [167,168]. It would be advantageous to continue such efforts with further computations of total cross sections Q_{if} as well as double differential cross sections $\mathrm{d}^2Q_{if}/(\mathrm{d}\theta_e\mathrm{d}E_e)$ for ionization in ion-tissue collisions. As usual, these latter distributions are obtained by integration of triple differential cross sections $\mathrm{d}^3Q_{if}/(\mathrm{d}\Omega_e\mathrm{d}E_e)$ over ϕ_e via the standard relationship:

$$\frac{\mathrm{d}^2Q_{if}}{\mathrm{d}\theta_e\mathrm{d}E_e} = \int_0^{2\pi} \mathrm{d}\phi_e \frac{\mathrm{d}^3Q_{if}}{\mathrm{d}\Omega_e\mathrm{d}E_e}, \tag{6.1}$$

$$\frac{\mathrm{d}^3Q_{if}}{\mathrm{d}\Omega_e\mathrm{d}E_e} \propto \left|T_{if}\right|^2, \quad \Omega = (\theta_e, \phi_e), \quad \theta_e \in [0, \pi], \quad \phi_e \in [0, 2\pi]. \tag{6.2}$$

Here, $T_{if} \equiv T_{if}(\Omega_e, E_e)$ is a quantum-mechanical transition amplitude for the passage of the system projectile-target from its initial to the final state, $i \longrightarrow f$. The CDW, CDW–EIS and MCB methods account fully for the ECC mechanism through the two-center problem by including the double continua of the ejected electron moving in the Coulomb fields of the projectile and target nuclei. As mentioned, the ECC effect does not yield a pronounced peak only in the angular distribution $\mathrm{d}^2Q_{if}/(\mathrm{d}\theta_e\mathrm{d}E_e)$ at $\theta_e \approx 0$ for $v \approx v_e$, but it also gives a cusp-shaped maximum in the single differential cross sections $\mathrm{d}Q_{if}/\mathrm{d}E_e$ at $v \approx v_e$:

$$\frac{\mathrm{d}Q_{if}}{\mathrm{d}E_e} = \int \mathrm{d}\Omega_e \frac{\mathrm{d}^3Q_{if}}{\mathrm{d}\Omega_e\mathrm{d}E_e}. \tag{6.3}$$

Neither of the said peaks in $\mathrm{d}Q_{if}/\mathrm{d}E_e$ and $\mathrm{d}^2Q_{if}/(\mathrm{d}\theta_e\mathrm{d}E_e)$ is obtained in the B1 method, which is a single-center theory for an electron which is described as moving only in the field of the target nucleus. In $\mathrm{d}Q_{if}/\mathrm{d}E_e$, both the B1 and CDW methods produce the so-called binary peak due to a direct collision of the incident ion with the target electron. Crucially, the CDW method satisfies the correct boundary conditions in the entrance and exit channels, as opposed to the B1 method. Especially important is the proper boundary condition in the final state because of the presence of three charged particles in the exit channel for ionization. Additionally, the final results for the fully quantum-mechanical transition amplitude $T_{if}^{(\mathrm{CDW})}$ regarding both ionization and electron capture in the case of arbitrarily complex atomic targets are given by analytical expressions. Such closed formulae can be readily used in e.g. simulations of the passage of ions through tissue. These essential improvements by means of an atomic physics theory derived from the first principles also obviate the need for resorting to empirical formulae for cross sections of limited validity for ions other than protons. One such fitting recipe is due to Rudd [153] who set up a phenomenological expression by adjusting the involved free parameters to approximately reproduce the available experimental data on proton-water collision. For other ions ($Z_\mathrm{P} > 1$), this latter formula relies upon the B1 method through its Z_P^2-scaling rule, which is not justified because of the missing ECC which scales like Z_P^3 [9,169]. Another prescription is the Hansen–Kocbach–Stolterfoht (HKS) formula [153] which modifies, in an empirical and artificial manner, the semi-classical version of the binary encounter approximation (BEA).

Close to the Bragg peak, the ions slow down considerably, and this increases enormously the probability for electron capture. As a matter of fact, the ions are brought to a complete stop at the Bragg peak (and, as such, are lost from the incident beam) by capturing one or more electrons to become neutral particles. Hence, any reliable computation of the stopping power must account for electron capture in the region near the Bragg peak [170–174]. This could hardly be accomplished by reliance upon the molecular version of the B1 approximation as recently was attempted in [175]. The B1 approximation for atomic targets has long been disqualified for charge exchange [7] due to the incorrect boundary conditions and the unphysical non-zero contribution of the inter-nuclear potential to the total cross sections. The same criticism can also be extended to the B1 approximation for electron capture from a molecular target [175]. To rescue the situation, here again the CDW methodologies are highly recommended by the intensive research in collisional phenomena in atomic physics, as recently reviewed in [3,4]. This should overcome the current empirical and phenomenological treatments of electron gain/loss by ion beams in particle transport through tissue. Thus far, rather than using the manageable atomic physics state-of-the-art methods for charge-changing processes in assessing the equilibrium balance between electron transfer to projectile and stripping of dressed/clothed projectile via electron loss (projectile ionization), researchers on stopping power opt to simulate such realistic phenomena by resorting to the Barkas Z_P^3-factor [176] with an empirical effective projectile charge dependent upon the incident velocity v [177].

6.6 Principal reasons for going beyond the first Born approximation

Thus far, cross sections Q and stopping powers $S(z)$ for ionization in particle-tissue collisions have been treated mainly through the Bethe–Bloch formula [16,17]. However, the Bethe–Bloch formula is only a high-energy simplification of the B1 method [11–15], which is itself known to be inadequate for ionization around and below the Massey peak for total cross sections [47,48]. As to differential cross sections, the B1 approximation has other drawbacks, such as the lack of the ECC effect and inability to quantitatively describe the electrons emitted in the forward and backward direction. Moreover, there are no Bethe–Bloch formulae for $\mathrm{d}^2Q_{if}/(\mathrm{d}\theta_e \mathrm{d}E_e)$ which are by far more important for transport of ions through tissue than the expressions for Q_{if} and $\mathrm{d}Q_{if}/\mathrm{d}E_e$. This is because the data on $\mathrm{d}^2Q_{if}/(\mathrm{d}\theta_e \mathrm{d}E_e)$ provide invaluable twofold information about the angular and energy distribution of ionized electrons. In contrast, the Bethe–Bloch stopping power formula is built only from the energy distribution based upon Q_{if} and/or $\mathrm{d}Q_{if}/\mathrm{d}E_e$. Furthermore, the original Bethe–Bloch formula is based exclusively on the channels of ionization and excitation, so that the corresponding stopping power scales as Z_P^2 with the projectile charge Z_P. It completely ignores electron capture and its significant role for the Bragg peak, which is clinically most important. It also neglects electron loss of dressed ions. Even for a hypothetically ideal beam comprised of nuclei alone, dressed ions such as hydrogenlike atomic systems are continuously formed along the primary beam track through electron capture from tissue by bare projectiles. Such clothed ions are short-lived and are destroyed by electron loss which is ionization of these ions in collisions with tissue. Because electron capture and electron loss processes occur interchangeably, charge-state equilibrium balance is quickly established. Plausibly, the lack of capture and electron loss are the main reasons for experimentally measured significant departures from the Z_P^2-scaling of the Bethe–Bloch formula. To cope with this situation, the mentioned empirical Barkas effect is invoked in modeling within particle transport physics in medicine and beyond. However, the Barkas effective charge cannot be derived from the first principles and, moreover, it has never been properly validated even within the B1 method for e.g. collisions between two hydrogenlike atomic systems.

6.7 Necessity for a molecular description of targets from tissue

The Bethe–Bloch formula includes the target structure in quite a crude way through certain shell effects and corrections due to binding energies, ionization potentials and the like. By contrast, the CDW methodologies employ two models for the target description based upon the atomic and molecular treatments [168]. The simplest atomic model is the Bragg sum rule [157] where a cross section $Q_{if}(\mathrm{M})$ for the transition $i \longrightarrow f$ of a molecular target M under impact of a projectile is obtained by computing the corresponding cross sections $Q_{if}(\mathrm{A}_n)$ for each of the constituent atoms $\{\mathrm{A}_n\}(1 \leq n \leq N)$ separately. Afterwards, the obtained separate atomic cross sections are added with the appropriate weight factors that are the number of the given atoms in the considered molecular target. Therefore, the Bragg sum rule takes no account of molecular bonding of atoms in a molecule. This additive rule is expected to be jus-

tified approximately only at sufficiently high energies at which the projectile passes quickly by the molecule and, thus, has no time to discern the internal structure of the target. Experimental data on e.g. atomic and molecular hydrogen H and H_2 indeed confirm this expectation. Namely, it has been found by measurements, that the cross sections $Q_{if}(H_2)$ for ionization and capture in collisions between fast protons and molecular hydrogens are nearly twice the corresponding data $Q_{if}(H)$ for the atomic hydrogen target, $Q_{if}(H_2) \approx 2Q_{if}(H)$. However, during the ending path of the passage of ions in tissue i.e. near the Bragg peak, the projectiles slow down considerably and this enhances their chance to be partially or completely neutralized via electron capture. Electron capture dominates over ionization at lower impact energies. At higher energies, the situation is precisely reverse, since the ionization cross section decreases slowly as $\propto (1/E)\ln E$ when the incident energy E is augmented, in contrast to a sharp $E^{-5.5}$-decline of the capture cross section, as predicted e.g. by the CDW method and confirmed experimentally.

At lower impact energies, in close vicinity to the Bragg peak where most of the dose is deposited to the tissue, it is anticipated that the Bragg sum rule will not be valid. This is because near the Bragg peak, the projectile has ample time to discern the molecular nature of the target, as opposed to a simple sum of the corresponding atomic constituents. In such a circumstance, a more adequate and complete description is necessary to account for chemical bondings of atoms in a molecular target. The needed description is given by a molecular model in which MO wave functions are used for a pure molecular target. In such a model, each MO is constructed as a linear combination of atomic orbitals (LCAO) in the form of e.g. Slater-type orbitals (STO) with the expansion coefficients $\{c_n\}$ obtained variationally by minimizing the expectation value of the given molecular Hamiltonian. Certain simplified versions of such approximate MOs [178,179] were used in the B1 [15,180] and CDW–EIS [167,168] methods applied to ionization of water by protons and alpha particles. Therefore, all the analytical results from e.g. the CDW, CDW–EIS and MCB methods for atomic targets can be used to arrive at the corresponding molecular version of these theories. Specifically, the entire molecular information of the target, no matter how complex it might be (including DNA), is stored in the expansion coefficients $\{c_n\}$ as well as in other variationally optimized parameters such as amplitudes and exponential decay factors $\{a_n, b_n\}$ as well as the orbital energies from the STOs. This implies that the key ingredients i.e the STOs are precisely of the same functional form as in the atomic model. Therefore, the whole calculation of distorted wave form factors from the molecular transition amplitudes $T_{if}(M)$ can be done analytically as in the atomic case. Hence the molecular transition amplitude $T_{if}(M)$ appears as a linear combination of atomic transition amplitudes $T_{if}(A_n)$ for the constituent atoms $\{A_n\}(1 \leq n \leq N)$ according to the following simple prescription:

$$T_{if}(M) = \sum_n c_n T_{if}(A_n). \tag{6.4}$$

This is an alternative kind of addition sum rule, hereafter called 'the transition amplitude sum rule' (or T-sum rule, for short), which can be employed to obtain the molecular data from the atomic ones. The T-sum rule differs fundamentally from the Bragg

sum rule, which adds the atomic cross sections to obtain the associated molecular data. By contrast, the T-sum rule carries out addition of the transition amplitudes which are complex-valued quantities and, as such, contain the vital phase interference of the constituent atomic form factors while taking the squared absolute value to deduce the differential cross section:

$$\frac{\mathrm{d}^3 Q_{if}(\mathrm{M})}{\mathrm{d}\Omega_e \mathrm{d}E_e} = \left|T_{if}(\mathrm{M})\right|^2 = \left|\sum_n c_n T_{if}(\mathrm{A}_n)\right|^2. \tag{6.5}$$

Such a phase interference information is completely missing from the sum of the cross sections in the Bragg sum rule:

$$\left\{\frac{\mathrm{d}^3 Q_{if}(\mathrm{M})}{\mathrm{d}\Omega_e \mathrm{d}E_e}\right\}_{\mathrm{Bragg}} = \sum_n w_n \frac{\mathrm{d}^3 Q_{if}(\mathrm{A}_n)}{\mathrm{d}\Omega_e \mathrm{d}E_e}. \tag{6.6}$$

Here, the nth Bragg expansion coefficient w_n is the given weighting factor determined by the concentration of the nth atom A_n in the molecule M. As such, the weights $\{w_m\}$ from the Bragg sum rule ignore chemical bondings of atoms in the considered molecule, as opposed to the T-sum rule where the molecular coefficients $\{a_n, b_n, c_n\}$ and the orbital energies truly account for such a bonding in a quantum-mechanical variational fashion.

6.8 Importance of relativistic effects

Light ions of impact energies $E \geq 350\,\mathrm{MeV/amu}$ used for radiotherapeutic treatment of deep seated tumors represent genuinely relativistic ions. Moreover, such relativistic ions produce fast δ-electrons from the domain of relativistic energies ($E_e \geq 100\,\mathrm{keV}$). Unlike non-relativistic high-energy electron capture, relativistic capture gives a non-negligible contribution compared to the relativistic ionization. Clearly, such an occurrence makes the use of relativistic theories indispensable for both ionization and electron capture [181–184]. The simple relativistic Bethe–Bloch formula for stopping power $S(z)$ involving ionization is already in use in the transport theory for energetic particles. However, this asymptotic formula suffers from the same basic defects as its non-relativistic counterpart enumerated above. The CDW theory for ionization can be generalized to relativistic energies similarly to relativistic electron capture [181–183]. The full relativistic treatment by means of the Dirac bound and continuum wave functions entails partial wave analysis in the Dirac-CDW method. Such a choice might be inconvenient for relativistic continuum wave functions for which the infinite sums over partial waves converge very slowly. This implies that too many transition amplitudes have to be computed to reach convergence by increasing the number of partial waves at high impact energies. However, Dirac wave functions are appropriate for the inner shells in heavy atoms for which full relativistic effects are important and must be taken into account as precisely as possible. This is not the case for hadron therapy where such heavy atoms are not encountered. Moreover

for multi-electron systems, the outer electrons give dominant contributions. For outer electronic shells, the relativistic effect play a minor role. As such, for radiotherapy with high-energy light ions, it would be fully sufficient to incorporate approximate relativistic effects through the Darwin and Sommerfeld–Mau wave functions for bound and continuum states, respectively [184]. Advantageously, these latter two functions do not necessitate the partial wave analysis. In this way the Darwin–Sommerfeld–Mau-CDW method would be obtained for electron capture as well as ionization and this would be an optimally practical relativistic theory for hadron therapy.

7 Improving Monte Carlo simulations by distorted wave theories

Once the cross sections for ionization and electron capture in fast ion-atom and ion-molecule collisions become available through the outlined strategy, simulation of transport of ions through tissue can be done by using stochastic simulations via MC codes, such as SHIELD-HIT [117,118] or other algorithms (FLUKA, GEANT4). The availability of the analytical formulae for cross sections in the CDW, CDW–EIS and MCB methods permits very fast pre-computations of the required atomic data bases that can be stored as numerical tables. Such tables would represent the readily accessible modules from which a direct sampling in MC codes could become feasible. With this setting of the interphase between the atomic data base modules and a selected MC code, the process of sampling itself would become practically instantaneous. Hence the possibility for an improved efficiency and accuracy of MC simulations. This is anticipated to be a significant step towards the sought 2% precision in the dose delivered at the tumor site.

8 Combined strategy for modeling ion transport in tissue-like media

We addressed some of the issues relevant to radiotherapy of deep seated tumors with protons and light ions of relativistic energies ($E \geq 350\,\text{MeV/amu}$). Our discussion has dealt mainly with the physics of atomic interactions of such ions with tissue. We highlighted the areas where the theoretical side of this problem can improve. Significant progress in this field critically depends upon the reliability of descriptions of transport of ions in tissue. These descriptions, in turn, rely heavily on the accurate data bases for cross sections and stopping powers computed by using the most adequate atomic physics theories. Starting from this initial premise, we illuminated a number of the directions that need significant improvements, such as:

(a) Going beyond several important insufficiencies of the first Born approximation and the Bethe–Bloch formula for energy losses by using the most adequate CDW methodologies from atomic collision physics.
(b) Employing single and double differential cross sections from the CDW theories and thus alleviating altogether the current overwhelming practice of resorting to some empirical, fitting formulae of limited validity.
(c) Surpassing the straightforward and frequently failing Bragg sum rule by employing the molecular description of molecular targets of tissue.

(d) Using relativistic version of the leading atomic physics methods for more adequate description of inelastic collisions.
(e) Providing highly accurate atomic data bases for cross sections and stopping powers in such a form which is readily accessible as precomputed modules for further sampling in MC simulations.

These features could significantly improve simulations of transport of ions in tissue by using e.g. the SHIELD-HIT code [116–118]. This MC algorithm employs an excellent nuclear data base due to the most accurate analyses from nuclear physics for precise modeling of nuclear collisions at the energies of interest ($E \geq 350$ MeV/amu) at which neutron losses represent the dominant channel in nuclear reactions. However, the corresponding atomic data base in SHIELD-HIT is rudimentary and restricted to the Bethe–Bloch formula for ionization and excitation losses, without any contribution from electron capture and ionization of dressed projectiles. The strategy proposed here should bridge this current gap between the nuclear and atomic physics in the SHIELD-HIT code [116–118]. Such an improvement is expected to represent a very important added value to stochastic simulations of transport of light ions in tissue for the purpose of radiotherapy of patients with deep seated tumors.

The anticipated spin-off from the suggested strategy is the possibility to make an objective assessment which could clarify the frequently alleged, but often unsubstantiated advantages of light ions relative to protons. The mentioned ongoing debates 'light ions versus protons' in Europe definitely need support in improving the existing lacunae in their 'pros and cons'. One of the goals of the presently proposed strategy could provide an impetus to help bridge this gap, as well. In particular, light ion therapeutic accelerators that are either under construction or planned to be built in several European countries will definitely need substantial improvement of atomic physics input for an overall successful modeling of the passage of these ions through tissue.[13]

9 Conclusion

Heavy ions find important applications across interdisciplinary fields including fusion research, space program, hadron therapy, etc. Particle transport physics is the chief common denominator in all these applications with atomic and nuclear collision physics as the principal ingredients. Detailed theoretical descriptions of the passage of ions through matter is customarily carried out by Monte Carlo (MC) simulations. Simpler problems could be amenable to analytical deterministic theories for particle transport in matter, like the Fokker–Planck simplification of the Boltzmann equation or sometimes even a single Gaussian from the Fermi–Eyges method and its extensions, but their usefulness becomes severely restricted by increased complexities of the investigated problems.

Complexities do not represent insurmountable obstacles to MC algorithms, that can, in principle, handle very difficult and involved geometries of the traversed medium. The more complex the problem, the more justified the use of MC simulations. Of

[13] A shorten version of our strategy from Sections 6–8 has first been published in 2004 [116] and was revisited more recently in 2009 [185].

course, MC modelings necessitate input cross sections that predominantly stem from deterministic theories for binary atomic and nuclear collisions. Moreover, the overall trust and adequacy of MC simulations depend critically on the accuracy and reliability of these input deterministic cross sections. Hence the deterministic-stochastic intertwining. Once equipped with the input cross sections, MC codes can begin to score the sought event histograms through statistical assessments of energy losses of the given incident, primary particles as well as their secondaries, tertiaries and particles of high-order generations. The MC simulations effectively approximate a true transport of ions through matter. Here, the prescribed event threshold for discriminating among various channels is used to predict whether the interaction at a considered point in space for the available energy would lead to nuclear transmutations or other types of nuclear reactions or to atomic transitions (excitation, electron capture, ionization or other atomic processes) through which energy loss of all the involved particles could occur. Various combination of nuclear and atomic collisions are also possible. In MC modelings, specific particle interactions could be conceived through e.g. ratios of various input cross sections, as done in e.g. MC code PENELOPE.

Evidently, there cannot be any substantial progress in studying ion transport phenomena by any MC algorithm without heavy reliance upon the most accurate data bases for cross sections from the first principle theories for atomic and nuclear collisions that determine the stopping powers for ions in their passage through matter.

In hadron therapy, thus far this was successfully accomplished for nuclear collisions using the most reliable and detailed data bases, but not sufficiently well for atomic collisions for which rather crude approximations are still overwhelmingly employed like the first Born approximation, the Bethe–Bloch formula, binary encounter approximation and some empirical ad hoc formulae with a number of fitting parameters. For example, the MC code SHIELD-HIT, which performs one of the most adequate stochastic simulations for ion transport in tissue-like materials, employs the best currently available data bases for cross sections from nuclear physics, but uses only the Bethe–Bloch formula for atomic cross sections for ion-water ionization. Similar uneven treatment of atomic and nuclear collisions is encountered also in other main MC codes such as FLUKA and GEANT4. The situation could be significantly improved by using the state-of-the-art distorted wave theories on atomic collisions without any adjustable parameters. Therefore, it would be important to apply these distorted wave methodologies to the major light ion beams ranging from protons to oxygen nuclei and to study these projectiles when they induce charge exchange, excitation and ionization of water molecule, which is one of the most essential tissue-equivalent targets. Water is the primary choice to study here, since this substance occupies 60-70% of the human body. Moreover, in practice within clinical dose planning systems, even when some other tissue-equivalent materials are used, the dose prescribed to the patient is ultimately standardized by being converted to the dose which would be equivalent to water as the traversed matter.

All the current main MC codes from particle transport physics in hadron therapy use the Bragg sum rule for obtaining molecular cross sections as the weighted sums of the involved atomic cross sections. This is crude, since such an approach ignores bondings in molecular targets. Existing experience from collision theories on molecular targets needs to be brought here, since distorted wave theories have already been applied to

high-energy ion-molecule collisions by expanding molecular orbitals in terms of linear combinations of atomic orbitals. There is yet another unexplored aspect of basic collision theory of high relevance to hadron therapy, and this is the influence of dynamic relativistic effects. Distorted wave relativistic collision theories were developed and implemented in atomic physics and should be exported to hadron therapy. The reason for pursuing this direction is in the fact that relativistic ion beams are used in radiotherapy for deep-seated tumor at a depth of the order of 25 cm. To penetrate to such depths, relativistic ion beams of about 200 MeV protons or 2100 MeV carbon nuclei are needed.

The next step for the needed critical improvement in theoretical descriptions of the passage of fast heavy ions through matter would be to incorporate the cross sections and stopping powers from high-energy atomic collisions treated by distorted wave theories into any of the available MC codes and, particularly, SHIELD-HIT algorithm would be recommended for this purpose in order to appropriately complement its already existing excellent counterpart from nuclear physics. Crucially, for completeness of the theory, transport of secondary δ-electrons should also be carried out together with ions. Fast ions create many energetic electrons by densely ionizing the targets. Due to their small mass, these electrons undergo multiple scattering and can contribute considerably to the total energy deposition in matter. In hadron therapy, among all the produced double strand breaks of DNA molecules of tissue, some 30 and 70% are due to direct hits of all ions (primaries, secondaries and, possibly, ions of higher-order generations) and δ-electrons, respectively. One of the most powerful MC codes in radiotherapy is SHIELD-HIT which, at present, transports only ions. On the other hand, electron transport is optimally modeled my MC code PENELOPE. Since all ions as well as secondary electrons produced by primary beams must ultimately be transported through tissue to fully and precisely account for the total dose, it would be highly desirable to build an interface which would connect SHIELD-HIT and PENELOPE.

The main impression which one has by comparing the developments of fast heavy ion collision theories and particle transport physics in radiotherapy is the natural connection of the main research themes. Yet the two disciplines proceed independently with minimal connections. This ought to be improved. But why should this be done, and what is really at stake here? Is it that medical physics is in need of more elaborated ion collision theories that, in turn, might not have much relevance for the dose planning and treatment systems and, hence, could lead only to more complicated, but no more useful clinical practice? The answer is in the very goal of particle transport physics in hadron therapy: to provide the most accurate estimates of total energy depositions in tissue without which there could be no reliable dose and treatment planning systems. And without the most accurate high-energy cross sections from the well-established distorted wave collision theories, there could be no substantial progress in particle transport physics in hadron therapy with the ensuing hindrance towards the corresponding dose and treatment planning systems in clinical protocols. Hence the *clinical need* for tightly connecting fast heavy ion collision theories with particle transport physics in radiotherapy.

Acknowledgments This work was supported by the Swedish Cancer Society Research Fund and King Gustav the Fifth's Jubilee Foundation.

References

1. Dž. Belkić, J. Comput. Meth. Sci. Eng. **1**, 1–74 (2001)
2. Dž Belkić, *Principles of Quantum Scattering Theory* (Institute of Physics Publishing, Bristol, 2004)
3. Dž. Belkić, *Quantum Theory of High-Energy Ion-Atom Collisions* (Taylor and Francis, London, 2008)
4. Dž. Belkić, I. Mančev, J. Hanssen, Rev. Mod. Phys. **80**, 249–314 (2008)
5. Dž. Belkić, Adv. Quantum Chem. **56**, 251–321 (2009)
6. I.M. Cheshire, Proc. Phys. Soc. **84**, 89–98 (1964)
7. Dž. Belkić, R. Gayet, A. Salin, Phys. Rep. **56**, 279–369 (1979)
8. Dž. Belkić, J. Phys. B **11**, 3529–3552 (1978)
9. Dž. Belkić, J. Phys. B **13**, L589–L593 (1980)
10. H.S.W. Massey, Rep. Prog. Phys. **12**, 248–269 (1949)
11. D.R. Bates, G.W. Griffing, Proc. Phys. Soc. A **66**, 961–971 (1953)
12. O. Boudrioua, C. Champion, C. Dal Cappello, Y.V. Popov, Phys. Rev. A **75**, 022720 (2007)
13. C. Champion, C. Dal Cappello, O. Boudrioua, H. Lekadir, Y. Sato, D. Ohsawa, Phys. Rev. A **75**, 032724 (2007)
14. C. Champion, O. Boudrioua, C. Dal Cappello, J. Phys. Conf. Ser. **101**, 012010 (2008)
15. C. Dal Cappello, C. Champion, O. Boudrioua, H. Lekadir, Y. Sato, D. Ohsawa, Nucl. Instr. Meth. Phys. Res. B **267**, 781–790 (2009)
16. H. Bethe, Ann. Phys. Lpz. **5**, 325–400 (1930)
17. F. Bloch, Ann. Phys. Lpz. **16**, 285–320 (1933)
18. G.B. Crooks, M.E. Rudd, Phys. Rev. Lett. **25**, 1599–1601 (1970)
19. M.W. Lucas, K.G. Harrison, J. Phys. B: Atom. Mol. Phys. **5**, L20–L22 (1972)
20. C.R. Vane, IEEE Trans. Nucl. Sci. **26**, 1078–1082 (1979)
21. W. Meckbach, I.B. Nemirovsky, C.R. Garibotti, Phys. Rev. A **24**, 1793–1802 (1981)
22. W. Meckbach, R. Vidal, P. Focke, I.B. Nemirovsky, E. Gonzalez-Lepera, Phys. Rev. Lett. **52**, 621–624 (1984)
23. P. Koschar, in *Forward Electron Ejection in Ion Collisions*, Book Series "Lecture Notes in Physics" (Springer, Berlin/Heidelberg, 1984), **213**, pp. 129–149
24. G.A. Glass, E. Peter, S.D. Berry, M. Breinig, R. Deserio, S.B. Elston, I.A. Sellin, Nucl. Instr. Meth. Phys. Res. B **10**, 138–141 (1985)
25. A. Skutlartz, S. Hagmann, H. Schmidt-Böcking, J. Phys. B: At. Mol. Opt. Phys. **21**, 3609–3618 (1988)
26. G.C. Bernardi, S. Suárez, P.D. Fainstein, C.R. Garibotti, W. Meckbach, P. Focke, Phys. Rev. A **40**, 6863–6872 (1989)
27. G. Bernardi, P. Focke, S. Suárez, W. Meckbach, Phys. Rev. A **50**, 5338–5341 (1994)
28. B. Fastrup, E. Horsdal-Pedersen, V.V. Afrosimov, A.A. Basalaev, M.N. Panov, in *21st International Conference on Physics of Electronic and Atomic Collisions, Sendai, Japan, July 21–27, 1999*, ed. by Y. Itikawa, K. Okuno, H. Tanaka, A. Yagishita, M. Matsuzawa, AIP Conference Proceedings, 500, vol. 2 (1999), p. 462
29. V.V. Afrosimov, A.A. Basalaev, B. Fastrup, E. Horsdal-Pedersen, K.V. Kashnikov, M.N. Panov, J. Phys. B: At. Mol. Opt. Phys. **33**, 4237–4242 (2000)
30. S. Hagmannn, I. Ali, Phys. Scr. **T80**, 329–330 (1999)
31. S. Hagmannn, I. Ali, H.-J. Lüdde, E. Wagner, http://www/jrm.phys.ksu.edu/Resource/Pubs/Progress/a-1-5.pdf
32. S. Hagmannn, I. Ali, http://www/jrm.phys.ksu.edu/Resource/Pubs/Progress/a-1-4.pdf
33. J. Fiol, S. Suaréz, D. Fregenal, A.D. González, P.D. Fainstein, Phys. Rev. **67**, 050702 (2003)
34. M.B. Shah, C. McGrath, C. Illescas, B. Pons, A. Riera, H. Luna, D.S.F. Crothers, S.F.C. O'Rourke, H.B. Gilbody, Phys. Rev. A **67**, 010704 (2003)
35. H. Schmidt-Böcking, L. Schmidt, Th. Weber, V. Mergel, O. Jagutzki, A. Czasch, S. Hagmann, R. Dorner, Y. Demkov, T. Jahnke, M. Prior, C.L. Cocke, T. Osipov, A. Landers, Rad. Phys. Chem. **71**, 627–632 (2004)
36. R.O. Barrachina, L. Sarkadi, Nucl. Instr. Meth. Phys. Res. B **233**, 260–265 (2005)
37. R.O. Barrachina, L. Sarkadi, Phys. Rev. A. **71**, 062712 (2005)

38. F. Afaneh, L.Ph.H. Schmidt, M. Schöffler, K.E. Stiebing, J. Al-Jundi, R. Dorner, J. Phys. B: At. Mol. Opt. Phys. **40**, 1745–1753 (2007)
39. S. Martínez, G. Bernardi, P. Focke, S. Suárez, D. Fregenal, J. Phys. B: At. Mol. Opt. Phys. **41**, 145204 (2008)
40. L. Sarkadi, A. Orbán, Phys. Rev. Lett. **100**, 133201 (2008)
41. L. Sarkadi, A. Orbán, Nucl. Instr. Meth. Phys. Res. B. **267**, 270–274 (2009)
42. E.H. Pedersen, L. Larsen, J. Phys. B: At. Mol. Opt. Phys. **12**, 4085–4098 (1999)
43. L. Gulyás, P.D. Fainstein, T. Shirai, J. Phys. B: At. Mol. Opt. Phys. **34**, 1473–1483 (2001)
44. M.E. Rudd, Y.-K. Kim, D.H. Madisson, T.J. Gray, Rev. Mod. Phys. **64**, 441–490 (1992)
45. N. Stolterfoht, R.D. DuBois, R.D. Rivarola, *Electron Emission in Heavy Ion-Atom Collisions* (Springer, Berlin, 1997)
46. D.S.F. Crothers, J.F. McCann, J. Phys. B **16**, 3229–3242 (1983)
47. P.D. Fainstein, V.H. Ponce, R.D. Rivarola, J. Phys. B **24**, 3091–3119 (1991)
48. S.F.C. O'Rourke, D.M. McSherry, D.S.F. Crothers, Adv. Chem. Phys. **121**, 311–356 (2002)
49. Dž. Belkić, Nucl. Instr. Meth. Phys. Res. B **124**, 365–376 (1997)
50. Dž. Belkić, J. Phys. B **30**, 1731–1745 (1997)
51. L.R. Dodd, K.R. Greider, Phys. Rev. **146**, 675–686 (1966)
52. L. Rosenberg, Phys. Rev. D **8**, 1833–1843 (1973)
53. A. Messiah, *Quantum Mechanics*, vol. 1 (Wiley, New York, 1966), p. 377
54. C.R. Garibotti, J.E. Miraglia, Phys. Rev. **21**, 572–580 (1980)
55. C.R. Garibotti, J.E. Miraglia, J. Phys. B **14**, 863–868 (1981)
56. C.R. Garibotti, J.E. Miraglia, Phys. Rev. A. **25**, 1440–1444 (1982)
57. L. Vainstein, L. Presnyakov, I. Sobelman, J. Exp. Theor. Phys. JETP. **18**, 1383–1385 (1964)
58. L. Vainstein, L. Presnyakov, I. Sobelman, Zh. Eksper. Teor. Fiz. **45**, 2015–2021 (1964)
59. L. Presnyakov, J. Exp. Theor. Phys. JETP. **20**, 760–761 (1965)
60. L. Presnyakov, Zh. Eksper. Teor. Fiz. **47**, 1134–1135 (1964)
61. D.P. Dewangan, B.H. Bransden, J. Phys. B **15**, 4561–4576 (1982)
62. M. Brauner, J.S. Briggs, H. Klar, J. Phys. B **22**, 2265–2287 (1989)
63. M. Brauner, J.S. Briggs, H. Klar, J.T. Broad, T. Rösel, K. Jung, H. Erhradt, J. Phys. B **24**, 657–673 (1991)
64. J. Berakdar, J.S. Briggs, H. Klar, Z. Phys. D **24**, 351–364 (1992)
65. F. Maulbetsch, J.S. Briggs, Phys. Rev. Lett. **68**, 2004–2006 (1992)
66. F. Maulbetsch, J.S. Briggs, J. Phys. B **26**, 1679–1696 (1993)
67. J. Berakdar, Phys. Rev. Lett. **72**, 3799–3802 (1994)
68. J. Berakdar, Phys. Rev. A **54**, 1480–1486 (1996)
69. S. Jones, D.H. Madison, Phys. Rev. Lett. **81**, 2886–2889 (2000)
70. S. Jones, D.H. Madison, Phys. Rev. A **62**, 042701 (2000)
71. L.J. Dubé, D.P. Dewangan, in *19th International Conference on the Physics of Electronic and Atomic Collisions*, Book of Abstracts, (Whistler, Canada, 1995), p. 62
72. S.F.C. O'Rourke, D.S.F. Crothers, J. Phys. B **30**, 2443–2454 (1997)
73. L. Gulyás, P.D. Fainstein, J. Phys. B **31**, 3297–3305 (1998)
74. M.F. Ciappina, W.R. Cravero, C.R. Garibotti, J. Phys. B **36**, 3775–3786 (2003)
75. M.F. Ciappina, W.R. Cravero, Braz. J. Phys. B **36**, 524–528 (2006)
76. S. Geltman, Proc. Phys. Soc. **75**, 67–76 (1960)
77. M.R.C. McDowell, J.H. Williamson, Phys. Lett. **4**, 159–161 (1963)
78. O. Belly, S.B. Schwartz, J. Phys. B **2**, 159–161 (1969)
79. R. Gayet, R. Janev, A. Salin, J. Phys. B **6**, 993–1002 (1973)
80. K.L. Bell, A.E. Kingston, P.J. Madden, J. Phys. B **11**, 3977–3982 (1978)
81. V. Sidis, C. Kubach, D. Fussen, Phys. Rev. A **27**, 2431–2446 (1983)
82. D. Fussen, W. Claeys, J. Phys. B **17**, L89–L93 (1984)
83. A.M. Ermolaev, J. Phys. B **21**, 81–101 (1988)
84. A.M. Ermolaev, C.J. Joachain, Phys. Rev. A **62**, 012710 (2000)
85. S. Lucey, C.T. Whelan, R.J. Allan, H.R.J. Walters, J. Phys. B **29**, L489–L495 (1996)
86. A.K. Kazansky, K. Taulbjerg, J. Phys. B **29**, 4465–4475 (1996)
87. B. Peart, D.S. Walton, K.T. Dolder, J. Phys. B **3**, 1346–1356 (1970)
88. D.S. Walton, B. Peart, K.T. Dolder, J. Phys. B **4**, 1343–1348 (1971)
89. B. Peart, R. Grey, K.T. Dolder, J. Phys. B **9**, 3047–3053 (1976)

90. K. Dolder, B. Peart, Rep. Progr. Phys. **48**, 1283–1332 (1985)
91. L.H. Andersen, D. Mathur, H.T. Schmidt, J. Vejby-Christensen, Phys. Rev. Lett. **74**, 892–895 (1995)
92. K. Fritioff, J. Sandström, P. Andersson, D. Hanstorp, F. Hellberg, R. Thomas, W. Geppert, M. Larsson, F. Österdahl, G.F. Collins, D.J. Pegg, H. Danared, A. Källberg, N.D. Gibson, Phys. Rev. A **69**, 042707 (2004)
93. Dž. Belkić, Phys. Rev. A **47**, 189–200 (1993)
94. Dž. Belkić, I. Mančev, V. Mergel, Phys. Rev. A **55**, 378–395 (1997)
95. R.J. Tweed, J. Phys. B **5**, 810–819 (1972)
96. C.J. Joachain, M. Terao, *Private Communication* (1991)
97. J. Silverman, O. Platas, F.A. Matsen, J. Chem. Phys. **32**, 1402–1406 (1960)
98. G.W.F. Drake, Nucl. Inst. Meth. Phys. Res. B **31**, 7–13 (1988)
99. I.S. Gradshteyn, I.M. Ryzhik, *Tables of Integrals, Series and Products* (Academic Press, New York, 1980)
100. J.D. Dollard, J. Math. Phys. **5**, 729–738 (1964)
101. F. Melchert, S. Krüdener, K. Huber, E. Salzborn, J. Phys. B **32**, L139–L144 (1999)
102. M. Rotenberg, J. Stein, Phys. Rev. **182**, 1–7 (1969)
103. S.S. Yu, B.G. Logan, J.J. Barnard, F.M. Bieniosek, R.J. Briggs, R.H. Cohen, J.E. Coleman, R.C. Davidson, A. Friedman, E.P. Gilson, L.R. Grisham, D.P. Grote, E. Henestroza, I.D. Kaganovich, M. Kireeff Covo, R.A. Kishek, J.W. Kwan, E.P. Lee, M.A. Leitner, S.M. Lund, A.W. Molvik, C.L. Olson, H. Qin, P.K. Roy, A. Sefkow, P.A. Seidl, E.A. Startsev, J-L. Vay, W.L. Waldron, D.R. Welch, Nucl. Fusion. **47**, 721–727 (2007)
104. G. Kraft, Prog. Part. Nucl. Phys. **45**, S473–S544 (2000)
105. G. Kraft, Nucl. Instr. Meth. Phys. Res. A **454**, 1–10 (2000)
106. M. Krämer, O. Jäkel, G. Kraft, D. Schardt, U. Weber, Phys. Med. Biol. **45**, 3299–3317 (2000)
107. M. Krämer, M. Scholz, Phys. Med. Biol. **45**, 3319–3330 (2000)
108. U. Amaldi, G. Kraft, Rep. Prog. Phys. **68**, 1861–1882 (2005)
109. T. Nakano, Y. Suzuki, T. Ohno, S. Kato, M. Suzuki, S. Morita, S. Sato, K. Oka, H. Tsujii, Clin. Cancer Res. **12**, 2185–2190 (2006)
110. D. Schulz-Ertner, O. Jäkel, W. Schlegel, Semin. Radiat. Oncol. **16**, 249–259 (2006)
111. D. Schulz-Ertner, H. Tsujii, J. Clin. Oncol. **25**, 953–964 (2007)
112. A. Porta, S. Agosteo, F. Campi, M. Caresana, Rad. Protect. Dosim. **132**, 29–41 (2008)
113. T. Bortfeld, Med. Phys. **24**, 2024–2033 (1997)
114. M. Hollmark, J. Uhrdin, Dž. Belkić, I. Gudowska, A. Brahme, Phys. Med. Biol. **49**, 3247–3265 (2004)
115. M. Hollmark, I. Gudowska, Dž. Belkić, A. Brahme, N. Sobolevsky, Phys. Med. Biol. **53**, 3477–3491 (2008)
116. Dž. Belkić, SHIELD-HIT: an optimal Monte Carlo code for simulations of transport of protons and heavier ions in tissue, Invited lecture, in: *Int. Conf. Comp. Math. Meth. Sci. Eng.*, Uppsala, Sweden, June 4–8, 2004, Proceedings (2004), ed. by E. Brändas, J. Vigo-Aguiar, pp. 10–16
117. I. Gudowska, N. Sobolevsky, P. Andreo, Dž. Belkić, A. Brahme, Phys. Med. Biol. **49**, 1933–1958 (2004)
118. O. Geithner, P. Andreo, N. Sobolevsky, G. Hartmann, O. Jäkel, Phys. Med. Biol. **51**, 2279–2292 (2006)
119. P. Andreo, Phys. Med. Biol. **55**, N205–N215 (2009)
120. P. Boyle, J. Ferlay, Ann. Oncol. **16**, 481–488 (2005)
121. *Technical Report Series*, No. 461, Vienna (2008)
122. B. Glimelius, A. Montelius, Radiother. Oncol. **83**, 105–109 (2007)
123. M. Lodge, M. Pijls-Johannesma, L. Stirk, A.J. Munro, D.D. Ruysscher, T. Jefferson, Radiother. Oncol. **83**, 110–122 (2007)
124. D.R. Olsen, Ø.S. Bruland, G. Frykholm, I.N. Norderhaug, Radiother. Oncol. **83**, 123–132 (2007)
125. O. Jäkel, B. Land, S.E. Combs, D. Schulz-Ertner, J. Debus, Radiother. Oncol. **83**, 133–138 (2007)
126. M. Brada, M. Pijls-Johannesma, D.D. Ruysscher, J. Clin. Oncol. **25**, 965–970 (2007)
127. J.E. Tepper, J. Clin. Oncol. **26**, 2436–2437 (2008)
128. H. Suit, H. Kooy, A. Trofimov, J. Farr, J. Munzenrider, T. DeLaney, J. Loeffler, B. Clasie, S. Safai, H. Paganetti, Radiother. Oncol. **86**, 148–153 (2008)
129. M. Goitein, J.D. Cox, J. Clin. Oncol. **26**, 175–176 (2008)
130. R.J. Schulz, A.R. Kagan, Int. J. Rad. Oncol. Biol. Phys. **72**, 1307–1309 (2008)
131. H. Suit, H. Kooy, Int. J. Rad. Oncol. Biol. Phys. **72**, 1309–1310 (2008)

132. K. Belkić, *Molecular Imaging Through Magnetic Resonance in Clinical Oncology* (Cambridge International Science Publishing, Cambridge, UK, 2003)
133. T. Bortfeld, Phys. Med. Biol. **51**, R363–R379 (2006)
134. W. Enghardt, P. Crespo, F. Fiedler, R. Hinz, J. Pawelke, F. Pönisch, Nucl. Instr. Meth. Phys. Res. A **525**, 284–288 (2004)
135. W. Enghardt, K. Parodi, P. Crespo, F. Fiedler, J. Pawelke, F. Pönisch, Radiother. Oncol. **73**, S96–S98 (2004)
136. F. Pönisch, K. Parodi, B.G. Hasch, W. Enghardt, Phys. Med. Biol. **49**, 5217–5232 (2004)
137. K. Parodi, H. Paganetti, H. Cascio, J.B. Flanz, A.A. Bonab, N.M. Alpert, K. Lohmann, T. Bortfeld, Med. Phys. **34**, 419–453 (2007)
138. R.R. Wilson, Radiology **47**, 487–491 (1946)
139. R.R. Wilson, Phys. Rev. **71**, 385–386 (1947)
140. C.A. Tobias, H.O. Anger, J.H. Lawrence, Am. J. Roentg. Rad. Ther. Nucl. Med. **67**, 1–27 (1952)
141. C.A. Tobias, J.E. Roberts, J.H. Lawrence, B.V. Low-Beer, H.O. Anger, J.L. Born, R. McCombs, C. Huggins, in Peaceful Uses of Atomic Energy, Proceedings of International Conference, Geneva (1955), pp. 95–106
142. L.I. Malis, R. Loevinger, L. Kruger, J.L. Rose, Science **126**, 302–303 (1957)
143. J.H. Lawrence, C.A. Tobias, J.L. Born, R. McCombs, J.L. Roberts, H.O. Anger, B.V. Low-Beer, C. Huggins, Cancer Res. **18**, 121–134 (1958)
144. B. Larsson, L. Leksell, B. Rexed, P. Sourander, W. Mair, B. Andersson, Nature **182**, 1222–1223 (1958)
145. B. Larsson, B.A. Kihlman, Int. J. Rad. Biol. **2**, 8–19 (1960)
146. A. Brahme, J. Nilsson, Dž. Belkić, Acta Oncol. **40**, 725–734 (2001)
147. Dž. Belkić, Adv. Quantum Chem. **51**, 157–233 (2006)
148. Dž. Belkić, K. Belkić, J. Math. Chem. **43**, 395–425 (2008)
149. Dž. Belkić, K. Belkić, J. Math. Chem. **45**, 563–597 (2009)
150. Dž. Belkić, K. Belkić, J. Math. Chem. **45**, 790–818 (2009)
151. Dž. Belkić, K. Belkić, J. Math. Chem. **45**, 819–858 (2009)
152. Dž. Belkić, Adv. Quantum Chem. **56**, 95–179 (2009)
153. Stopping powers and ranges for protons and alpha particles, *ICRU Report 49: International Commission of Radiation Units and Measurements* (Barthesda, MD, USA, 1993)
154. Stopping powers and ions heavier than helium, *ICRU Report 73: International Commission of Radiation Units and Measurements* (Oxford University Press, 2005)
155. W.H. Bragg, Phil. Mag. **8**, 719–725 (1904)
156. W.H. Bragg, R.D. Kleeman, Phil. Mag. **8**, 726–738 (1904)
157. W.H. Bragg, R.D. Kleeman, Phil. Mag. **10**, 318–340 (1905)
158. A. Lomax, Phys. Med. Biol. **44**, 185–205 (1999)
159. L. Cella, A. Lomax, R. Miralbell, Phys. Medica **17**(Supplement 1), S100–S102 (2001)
160. A.J. Lomax, T. Boehringer, A. Coray, E. Egger, G. Goitein, M. Grossmann, P. Juelke, S. Lin, E. Pedroni, B. Rohrer, W. Roser, B. Rossi, B. Siegenthaler, O. Stadelmann, H. Stauble, C. Vetter, L. Wisser, Med. Phys. **28**, 317–324 (2001)
161. W.R. Hendee, Med. Phys. **26**, 1185–1187 (1999)
162. R.J. Schulz, Med. Phys. Lett. Ed. **26**, 2515 (1999)
163. A.J. Lomax, Med. Phys. Lett. Ed. **27**, 622–623 (2000)
164. H. Tsujii, T. Bortfeld, Radiother. Oncol. **58**, S72 (2001)
165. M.A. Chaudhri, Radiother. Oncol. **58**, S22 (2001)
166. M.A. Chaudhri, **600**, 49–51 (2001)
167. G.H. Olivera, A.E. Martínez, R.D. Rivarola, P.D. Fainstein, Rad. Res. **144**, 241–247 (1995)
168. G.H. Olivera, P.D. Fainstein, R.D. Rivarola, Phys. Med. Biol. **41**, 1633–1647 (1996)
169. G.C. Bernardi, P.D. Fainstein, C.R. Garibotti, S. Suárez, J. Phys. B **23**, L139–L143 (1990)
170. A. Dalgarno, G.W. Griffing, Proc. Phys. Soc. A **232**, 423–434 (1955)
171. A. Dalgarno, G.W. Griffing, Proc. Phys. Soc. A **248**, 415–428 (1958)
172. P.D. Fainstein, V.H. Ponce, A.E. Martínez, Phys. Rev. A **47**, 3055–3061 (1993)
173. G.H. Olivera, A.E. Martínez, R.D. Rivarola, Phys. Rev. A **49**, 603–606 (1994)
174. A.E. Martínez, R.D. Rivarola, P.D. Fainstein, Nucl. Instr. Meth. B **111**, 7–11 (1996)
175. S. Houamer, Yu.V. Popov, C. Dal Cappello, C. Champion, Nucl. Instr. Meth. Phys. Res. B **267**, 802–806 (2009)

176. W.H. Barkas, *Nuclear Research Emulsions*, vol. 1 (Academic Press, New York, 1963)
177. L.E. Porter, Adv. Quantum Chem. **46**, 91–119 (2004)
178. R. Moccia, J. Chem. Phys. **40**, 2186–2192 (1964)
179. K. Siegbahn, C. Nordling, G. Johansson, J. Hedman, P.F. Hedén, K. Hamrin, U. Gelius, T. Bergmark, L.O. Werme, R. Manne, Y. Baer, *ESCA Applied to Free Molecules* (North-Holland, Amsterdam, 1969)
180. B. Senger, R.V. Rechenmann, Nucl. Instr. Meth. Phys. Res. B **2**, 204–207 (1984)
181. J.F. McCann, J. Phys. B **18**, L569–L573 (1985)
182. G.R. Deco, R.D. Rivarola, J. Phys. B **19**, 1759–1770 (1986)
183. G.R. Deco, R.D. Rivarola, J. Phys. B **20**, 5125–5177 (1987)
184. G.R. Deco, P.D. Fainstein, R.D. Rivarola, Nuc. Instr. Meth. B **35**, 100–102 (1988)
185. Dž. Belkić, Review of leading theories for high-energy heavy particle collisions with prospects for applications to medicine, Invited lecture, *The 6th Int. Conf. on "Radiation Damage in Biomolecular Systems" (RADAM)*, Frankfurt, Germany, July 1–5, 2009. Book of Abstracts (Frankfurt Institute for Advanced Studies (FIAS), Goethe University, 2009), ed. by Solov'yov, pp. 48–49 (http://fias.uni-frankfurt.de/radam2009)